J. Fluid Mech. (1986), *vol.* 170, *pp.* 199–232
Printed in Great Britain

The hydrodynamic stability of flow over Kramer-type compliant surfaces. Part 2. Flow-induced surface instabilities

By P. W. CARPENTER
Department of Engineering Science, University of Exeter, Exeter

AND A. D. GARRAD
Garrad Hassan and Partners, 10 Northampton Square, London EC1M 5PQ

(Received 15 May 1985)

The flow-induced surface instabilities of Kramer-type compliant surfaces are investigated by a variety of theoretical approaches. This class of instability includes all those modes of instability for which the mechanism of generation involves essentially inviscid processes. The results should be applicable to all compliant surfaces that could be modelled theoretically by a thin elastic plate, with or without applied longitudinal tension, supported on a springy elastic foundation, with or without a viscous fluid substrate; material damping is also taken into account through the viscoelastic properties of the solid constituents of the coatings.

The simple case of a potential main flow is studied first. The eigenmodes for this case are subjected to an energy analysis following the methods of Landahl (1962). Instabilities that grow both in space and time are then considered, and absolute and convective instabilities identified and analysed.

The effects of irreversible processes on the flow-induced surface instabilities are investigated. The shear flow in the boundary layer gives rise to a fluctuating pressure component which is out of phase with the surface motion. This leads to an irreversible transfer of energy from the main stream to the compliant surface. This mechanism is studied in detail and is shown to be responsible for travelling-wave flutter. Simple results are obtained for the critical velocity, wavenumber and stability boundaries. These last are shown to be in good agreement with the results obtained by the numerical integration of the Orr–Sommerfeld equation. An analysis of the effects of a viscous fluid substrate and of material damping is then carried out. The simpler inviscid theory is shown to predict values of the maximum growth rate which are, again, in good agreement with the results obtained by the numerical integration of the Orr–Sommerfeld equation provided that the instability is fairly weak.

Compliant surfaces of finite length are analysed in the limit as wave-length tends to zero. In this way the static-divergence instability is predicted. Simple formulae for critical velocity and wavenumber are derived. These are in exact agreement with the results of the simpler infinite-length theory. But, whereas a substantial level of damping is required for the instability on a surface of infinite length, static divergence grows fastest in the absence of damping on a surface of finite length.

1. Introduction

The quest for drag reduction and turbulence suppression may be the practical motivation for the current research on compliant surfaces, but it is the profusion of

potential modes of instability that makes the hydrodynamic stability of such surfaces a challenging and interesting problem. Of course, the identification and prediction of these instabilities should also be of considerable practical concern if substantial transition delays or turbulence suppression are ever to be achieved with real compliant surfaces. In fact, it seems quite likely that the occurrence of unexpected and unwanted instabilities has been an important factor in frustrating past attempts to achieve repeatable drag reductions.

Why, then, is the flow over compliant surfaces susceptible to so many different types of instability? The simple answer is that the dynamic system in question consists of two coupled wave-bearing media – the flowing fluid and solid flexible wall. In this respect the situation is similar to water waves. The structure of compliant surfaces is considerably more complex than water, however, which greatly increases the chances of additional modes of instability. The complexity of the problem can be appreciated by studying the simple model problem of potential flow over a compliant surface consisting of a plate or tensioned membrane supported on a continuous elastic foundation. In this case, it can be readily shown that three distinct types of travelling wave may occur. Each of these responds differently to the presence of a boundary layer and to viscous and material damping. Moreover, the possibility of modal interaction and coalescence with the Tollmien–Schlichting waves also exists.

The profusion of instabilities was fully appreciated in the earliest theoretical analyses by Benjamin (1960) and Landahl (1962) which closely followed publication by Kramer (1960) of his pioneering experimental work on compliant coatings. Originally, Benjamin (1960) identified three types of instability. The first type, Tollmien–Schlichting waves, are similar to those found in flows over rigid walls, but modified by surface flexibility. Viscous effects play an essential role in their generation. The second type comprise surface waves travelling at speeds close to the free wave speed of the flexible surface. The mechanism of generation of this type of wave was studied earlier by Benjamin (1959) and Miles (1957). A shear layer is necessary for the waves to grow but, apart from that, viscosity does not play an essential role. The third type was termed a Kelvin–Helmholtz instability. These instabilities can exist with inviscid and even potential flow, as shown by Miles (1959*b*), for example.

Later, Landahl (1962) and Benjamin (1963) showed that the dynamic system comprising an inviscid shear layer flowing over a compliant surface could support three distinct classes of wave rather than two. These could be classified according to whether their existence led to a decrease, increase or to no change in the total energy of the system. Class-A waves are associated with a fall in energy and are destabilized by damping; in this respect Tollmien–Schlichting waves can be considered as belonging to this category. Class-B waves are associated with a rise in energy and are stabilized by damping. These are really the same as the second type of wave originally identified by Benjamin (1960). Finally, Class C are associated with no change in energy level and are unaffected by damping. The Kelvin–Helmholtz instability belongs to this class.

In Part 1 {Carpenter & Garrad (1985) hereinafter referred to as I} of the present work, Benjamin and Landahl's classification of instabilities was not followed for various reasons. Instead, two broad categories of instabilities were defined. The first was termed Tollmien–Schlichting instabilities (TSI); and the second category was called flow-induced surface instabilities (FISI), consisting of all those instabilities which could exist if the viscous boundary layer were replaced by an inviscid shear layer. It was recognized that to some extent the distinction is rather artificial,

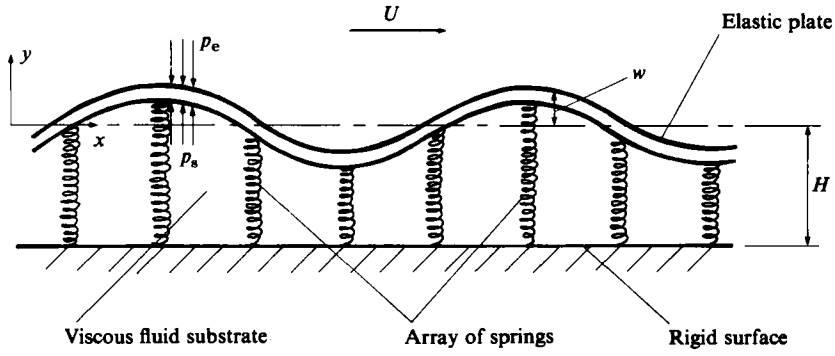

FIGURE 1. A schematic illustration of the theoretical model for a compliant surface.

especially as under certain circumstances the TSI can interact and coalesce with one of the FISI modes. However, it has proved very useful in practice to develop a separate inviscid treatment for the FISI associated with Kramer-type compliant surfaces. This term is used, as in I, for compliant coatings which can be modelled by an elastic plate or tensioned membrane supported on a continuous springy elastic foundation with or without a viscous fluid substrate (see figure 1). This treatment is the main subject of the present paper; some preliminary results have already appeared in Carpenter & Garrad (1982) and Carpenter (1984*a*, *b*). Part 1 (I) dealt with the TSI and Part 3 will consider the interaction and coalescence of the TSI and FISI modes; a preliminary version of this latter work was given by Carpenter, Gaster & Willis (1983).

For a potential flow over a non-dissipative Kramer-type surface it will be shown below that there are three classes of waves, as found by Landahl and Benjamin. However, when a more realistic model is considered, it appears that only the Class-B wave – here renamed travelling-wave flutter (TWF) – occurs as a travelling wave. The Class-A wave gives way to another type of instability, namely static divergence. As its name suggests this instability does not take the form of a travelling wave but rather exists as a periodic series of humps and valleys. Divergence does not fit readily into Benjamin and Landahl's classification scheme. Thus, four types of instability appear to be possible in a realistic model of flow over Kramer-type compliant surfaces. These comprise the TSI, TWF and static divergence; and the combined instability formed by the coalescence of the TSI and TWF.

A variety of theoretical approaches have been applied to FISI on compliant surfaces. These can be sorted into five loose categories, namely: (i) the hydro/aero-elastic approach (e.g. Landahl 1962; Benjamin 1963; Dowell 1971, 1975; Kornecki 1978; Carpenter & Garrad 1982; Garrad & Carpenter 1982*a*, *b*); (ii) use of the negative-energy concept (e.g. Landahl 1962, 1964; Benjamin 1963); (iii) analogies with water waves (e.g. Benjamin 1960, 1963, 1964); (iv) numerical solution of the Orr–Sommerfeld equation (e.g. Carpenter & Garrad 1985; Carpenter *et al.* 1983; Carpenter 1984*a*); (v) the causal approach (e.g. Brazier-Smith & Scott 1984; Atkins 1982). Each of these various approaches has elucidated some aspect of this complex problem but the overall picture is, perhaps, somewhat confusing. It is the main aim of the present paper to bring together all the previous approaches in order to present a consistent overall account of the FISI on Kramer-type compliant surfaces. Accordingly, rather than reviewing the relevant literature at this juncture, it is more convenient to discuss the work of previous investigators at appropriate points in the

main text. Two very recent reviews on the subject have been given by Gad-el-Hak (1986*b*) and Dowell (1985).

The present paper is organized as follows. Section 2 contains an analysis of the instabilities for a potential flow over a compliant surface. It has three subsections: in §2.1 the basic theory is developed; and the energy analysis of the instabilities due to Landahl (1962) and Benjamin (1963) is briefly described and discussed in §2.2. The concepts of convective and absolute temporal instabilities are investigated in §2.3. A fairly detailed comparison is made between the results of the present theory and those of the causal theory due to Brazier-Smith & Scott (1984). The effects of irreversible processes on the FISI are analysed in §3. Boundary-layer effects are considered in §3.1 and the effects of viscous and viscoelastic damping in §3.2. Section 4 is devoted to the treatment of static divergence. The analysis for a surface of finite length is presented for the limiting case of wavelength tending to zero.

The overall conclusions are given in §5. In addition, the various theoretical results are applied to the original Kramer coatings with the same objective as I, namely to ascertain whether Kramer's experimental observations were consistent with his view that transition delay was responsible for the drag reductions achieved in his tests. The Kramer coatings are also chosen as a suitable example to illustrate the theory in the main body of the paper. It should be emphasized, however, that Kramer's experiments are not regarded as 'bench-mark' tests and the comparison between theoretical predictions and his experimental observations are not considered to constitute, in any sense, a verification of the theory.

2. Potential main flow

2.1. *Basic theory*

A potential main flow over a non-dissipative compliant surface, comprising a thin plate or a tensioned membrane, supported on an elastic foundation, represents the simplest model of flow over a compliant surface. Many important features, which are also exhibited by more realistic models, can be readily demonstrated with this simple system. The results need to be interpreted with great care, however, because this simple system turns out to be an almost pathological approximation in that it appears to give the incorrect result as regards stability under virtually any limiting process. For example, it will be shown below that it does not agree with the results obtained when internal damping tends to zero. In §3.1 it will be shown that the stability predictions do not agree with those obtained in the limit as boundary-layer thickness tends to zero. Finally, it is found in §4 that for a surface of finite length in the limit as instability wavelength tends to zero the results obtained are once again at variance with those obtained by the simple model.

For a two-dimensional travelling wave the surface displacement takes the form

$$w = w_0 \exp\{\mathrm{i}\alpha(x-ct)\}, \tag{2.1}$$

where α is the wavenumber, $c = c_\mathrm{r} + \mathrm{i}c_\mathrm{i}$ is the complex wave speed, x is the streamwise coordinate and t is time. The surface motion is governed by the following equation (see I):

$$\rho_\mathrm{m} b \frac{\partial^2 w}{\partial t^2} + d\frac{\partial w}{\partial t} + B\frac{\partial^4 w}{\partial x^4} - T\frac{\partial^2 w}{\partial x^2} + K_\mathrm{E} w = \delta p_\mathrm{s} - \delta p_\mathrm{e}, \tag{2.2}$$

where ρ_m and b are respectively the density and thickness of the plate, d is a damping coefficient, B and T are respectively the flexural rigidity of and tension per unit width

applied to the plate, δp_s and δp_e are the perturbations in dynamic pressure in the substrate fluid and main stream respectively, K_E is an equivalent spring stiffness incorporating the effects of perturbations to hydrostatic pressure difference, given by

$$K_E = K - g(\rho_e - \rho_s), \tag{2.3}$$

where K is the spring stiffness, g is the acceleration due to gravity, and ρ_e and ρ_s are respectively the densities of the mainstream and substrate fluids.

In the present section the main flow will be taken to be potential and the substrate fluid assumed to be absent, so that

$$\delta p_e = -\rho_e \alpha (U_\infty - c)^2 w, \quad \delta p_s = 0, \tag{2.4}$$

where U_∞ is the free-stream velocity. If (2.1) and (2.4) are substituted into (2.2) the following non-dimensional characteristic equation (dispersion relation) for complex wave speed can be derived:

$$\bar{c}^2 - \bar{c}_0^2 + C_A(1-\bar{c})^2 + \mathrm{i} C_D \bar{c} = 0, \tag{2.5}$$

where $\bar{c} = \bar{c}_r + \mathrm{i}\bar{c}_i$ and $\bar{c}_0$ are the complex wave speed and free wave speed respectively divided by U_∞, $C_A = \rho_e/(b\rho_m \alpha)$ and $C_D = d/(\alpha \rho_m b U_\infty)$;

$$c_0 = \left\{\frac{B\alpha^2 + T + K_E \alpha^{-2}}{(b\rho_m)}\right\}^{\frac{1}{2}} \tag{2.6a}$$

and

$$\bar{c}_0 = \{C_B^* C_A^{-2} + C_T^* + C_K^* C_A^2\}^{\frac{1}{2}}, \tag{2.6b}$$

where

$$C_B^* = \frac{B\rho_e^2}{\rho_m^3 b^3 U_\infty^2}, \quad C_T^* = \frac{T}{\rho_m b U_\infty^2}, \quad C_K^* = \frac{\rho_m b K_E}{\rho_e^2 U_\infty^2}. \tag{2.7}$$

When damping is absent (2.5) is a quadratic in terms of $\bar{c}$, the roots of which are given by

$$\bar{c} = \frac{C_A}{1+C_A}\left(1 \pm \frac{U^*}{U_\infty}\right), \tag{2.8}$$

where

$$U^* = \left\{\frac{(1+C_A)}{C_A} c_0^2 - \frac{1}{C_A} U_\infty^2\right\}^{\frac{1}{2}}.$$

The relationship between wavenumber and complex wave speed determined by (2.8) is illustrated in figure 2 where the results correspond to Kramer's coating C (the one with the best performance – see I) at a speed of 25 m/s. It can be seen in figure 2 that for low wavenumbers there are two distinct families of wave. Branch FH corresponds to a fairly fast wave which travels downstream. The other branch corresponds to an upstream-travelling wave between C and D and a relatively slow downstream-travelling wave between D and F. At intermediate wavenumbers between F and G the two families of wave coalesce, only to bifurcate again at G. When damping is absent the system is only unstable for branch FG, as can be seen from the curve for $\bar{c}_i$. Outside this limited range of wavenumbers the system is neutrally stable; $\bar{c}_i$ is not plotted in figure 2 where it is zero. Thus, in total, there are three types of wave – the fast wave corresponding to FH and BG, the slow or upstream-travelling wave corresponding to FDC and AG, and the unstable wave corresponding to FG formed by the coalescence of the other two types.

When damping is present the roots of (2.5) are given by

$$\bar{c} = \frac{C_A}{1+C_A}\left\{1 \mp \frac{C_A C_D^*}{2\bar{c}_0 \Delta}\right\} + \mathrm{i}\frac{\bar{c}_0}{1+C_A}\left\{-\frac{C_A C_D^*}{2\bar{c}_0} \pm \Delta\right\}, \tag{2.9}$$

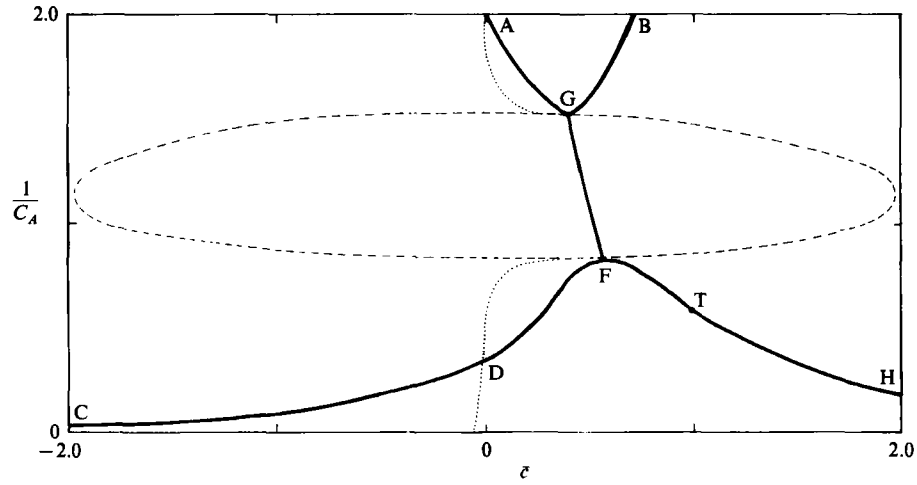

FIGURE 2. Non-dimensional wavenumber vs. non-dimensional wave speed. $C_B^* = 0.109$, $C_T^* = 0$, $C_K^* = 0.327$. ——, $\bar{c}_r$; – – – –, $\bar{c}_i : C_D^* = 0$; . . . . . , $\bar{c}_i : C_D^* = 0.01$.

where

$$\Delta = \frac{1}{\sqrt{2}}\left[\left\{\left(1 + C_A - \frac{C_A}{\bar{c}_0^2} - \frac{C_A^2 C_D^*}{4\bar{c}_0^2}\right)^2 + \left(\frac{C_A C_D^*}{\bar{c}_0^2}\right)^2\right\}^{\frac{1}{2}} - 1 - C_A + \frac{C_A}{\bar{c}_0^2} + \frac{C_A^2 C_D^{*2}}{4\bar{c}_0^2}\right]^{\frac{1}{2}}$$

and

$$C_D^* = d/\rho_e U_\infty.$$

Equation (2.9) is similar to, but not identical with, results given by Landahl (1962) and Kornecki (1978). From (2.9) it can be seen that the onset of instability occurs when $2\Delta = C_A C_D^*/\bar{c}_0$. By examining the real part of $\bar{c}$ in (2.9) it can be seen that this instability condition corresponds to $\bar{c} = 0$. Thus points D and A (rather than F and G) in figure 2 mark the onset of instability whenever damping, no matter how light, is present. The unstable branch of $\bar{c}_i$ is plotted in figure 2 for a value of $C_D^* = 0.01$; $\bar{c}_r$ is virtually unchanged from its value for $C_D^* = 0$.

For a fixed wavenumber the velocity for which $\bar{c} = 0$ is given by $\bar{c}_0 = C_A^{\frac{1}{2}}$, or

$$U_\infty = \frac{c_0}{C_A^{\frac{1}{2}}}, \tag{2.10}$$

so differentiating the right-hand side of (2.10) with respect to α and setting the result equal to zero leads to the critical wavenumber, which is given by

$$\alpha_d = \left\{\frac{(T^2 + 12BK_E)^{\frac{1}{2}} - T}{6B}\right\}^{\frac{1}{2}}. \tag{2.11}$$

For the special cases of the untensioned plate and the tensioned membrane (2.11) reduces to

$$\alpha_d = \left(\frac{K_E}{3B}\right)^{\frac{1}{4}}, \quad \alpha_d = \left(\frac{K_E}{T}\right)^{\frac{1}{2}} \tag{2.12}$$

respectively. The corresponding critical velocity is found by substituting (2.11) into (2.10). In the two special cases, substitution of (2.12) into (2.10) gives

$$U_d = 2\left\{\frac{BK_E^3}{27\rho_e^4}\right\}^{\frac{1}{8}}, \quad U_d = \left\{\frac{4K_e T}{\rho_e^2}\right\}^{\frac{1}{4}} \tag{2.13}$$

respectively.

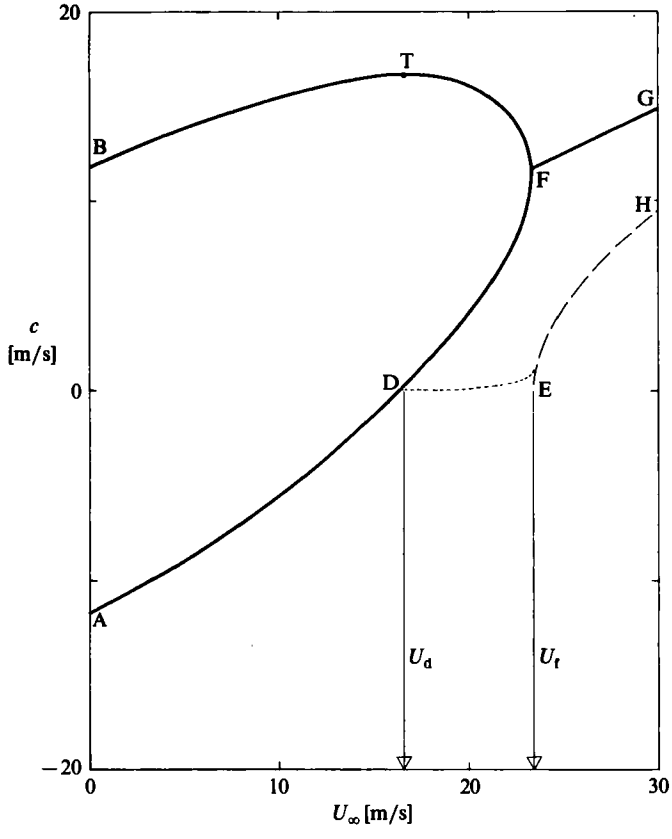

FIGURE 3. Complex wave speed vs. free-stream speed for $\alpha = \alpha_d$ – Kramer's best case. $C_B^* = 68.13/U_\infty^2$, $C_T^* = 0$, $C_K^* = 204.4/U_\infty^2$. ——, c_r; — —, c_i: $C_D^* = 0$; - - - - - - -, c_i: $C_D^* = 0.25/U_\infty$.

In (2.11)–(2.13) the critical wavenumbers and velocities have been denoted by the subscript d. This is because the instability is usually identified as a divergence. Actually, as can be seen from figure 2, the theory indicates that the instability is a slowly travelling wave and not static divergence. It will be shown in §3 that when boundary-layer effects are taken into account this slowly travelling wave is stabilized for low levels of damping. However, in §4 it will be shown that for surfaces of finite length a true divergence-type instability does occur, but the critical velocity and wavenumber are still given by (2.13) and (2.11) respectively, in the limit as wavelength tends to zero.

The onset of instability is probably best illustrated by plotting the complex wave speed c against the free-stream velocity U_∞ as in figure 3. In this case the wavenumber is given the value determined by (2.12) and the values of c obtained from (2.8) or (2.9). The results presented in figure 3 are for the mechanical properties, i.e. values of B, T, K_E etc. which correspond to the Kramer coating with the best performance (i.e. elastic modulus, $E = 0.5\ \mathrm{N/mm^2}$, see I). Since in practice the mechanical properties do not vary with U_∞, the non-dimensional coefficients C_B^*, C_K^* and C_D are first evaluated at a reference velocity of 25 m/s and then multiplied by the factors $(25/U_\infty)^2$ or $(25/U_\infty)$ as appropriate. Thus the dispersion relation illustrated in figure 2 corresponds to a free-stream speed of 25 m/s in figure 3.

The features displayed in figure 3 reflect those that appear in figure 2. For example,

in the absence of damping, there are two separate neutrally stable waves for $U_\infty < U_f$ – the so-called flutter speed – corresponding to ADF and BTF in figure 3. It can easily be shown from (2.8) that when $\alpha = \alpha_d$

$$U_f = U_d(1+C_A)^{\frac{1}{2}}. \tag{2.14}$$

For $U_\infty > U_f$ the two waves coalesce and a severe flutter-type instability sets in, corresponding to FG and EH in figure 3. When damping is present instability† first occurs when U_∞ reaches U_d which. again, mirrors what is shown in the dispersion relation of figure 2.

The sudden reduction in critical velocity from U_f to U_d when damping is introduced was once regarded as rather paradoxical by aeroelasticians. The phenomenon was first fully explained by Landahl (1962). He showed that in a condition of neutral stability the destabilizing hydrodynamic and inertial forces are exactly balanced by the restoring mechanical forces in the surface. The main effect of damping is to slow down the wave slightly. This slight reduction in phase speed will leave the restorative mechanical force unchanged but the destabilizing hydrodynamic and inertial forces will be slightly changed. For the wave regime denoted by AD in figure 3 the destabilizing forces are reduced so that damping is stabilizing. On the other hand for regimes DF and BF the destabilizing forces are increased so that damping is destabilizing.

The explanation summarized above is expressed in the simplest possible terms. There is, however, a more fundamental approach to the question involving an analysis of the changes in energy associated with a particular wave. This approach also originated with Landahl (1962), and is considered in the next section.

2.2. *An energy analysis of the waves*

Landahl (1962) and Benjamin (1963) showed how the effects of irreversible processes on the stability of the FISI on compliant surfaces could be predicted by means of a careful analysis of the change in total energy level associated with the wave in question. Moreover, with this approach it is only necessary to know the solution to the corresponding non-dissipative problem. Thus, by use of the simple solution (2.8), an energy analysis can predict the effects on stability of viscous and viscoelastic damping and of the boundary layer. The analysis given below is based on that given by Benjamin who generalized and extended Landahl's original analysis.

When U^* is real the solutions (2.8) correspond to neutrally stable waves which therefore cannot grow in amplitude. Imagine. however, that some unspecified external agency exists whereby the waves are made to grow gradually until a steady state is reached and subsequently maintained. The key question is: How much energy must be expended by this unspecified external agency to bring about this state of affairs?

To answer this question Landahl and Benjamin calculated the kinetic energy $\overline{E}_k$ and the potential (strain) energy $\overline{E}_p$ of the compliant surface in the final steady state. Both types of energy are averaged over a wavelength. But $\overline{E}_k + \overline{E}_p$ is not the energy which must be supplied by the external agency, because energy is extracted from the main stream by the work done on the surface by the hydrodynamic pressure forces during the development of the wave. Accordingly, making the assumption of an unsteady potential flow, the total work $\overline{W}$ done by hydrodynamic pressure on the surface during the development of the wave was evaluated and averaged over a

† In figure 3 c_i is only plotted when it is positive, i.e. for an instability.

wavelength. Thus the net energy required from the external agency in order to create a given wave is given by

$$E_A = \overline{E}_p + \overline{E}_k - \overline{W}. \tag{2.15}$$

Benjamin called this quantity the activation energy, and by use of the simple solution (2.8) showed that

$$E_A \propto U^*(U^* \pm U_\infty). \tag{2.16}$$

Landahl and Benjamin defined three main classes of wave, namely those for which

(i) $E_A < 0$: Class A,

(ii) $E_A > 0$: Class B,

(iii) $E_A = 0$: Class C.

At first sight, perhaps, it may seem rather paradoxical to propose the existence of waves having negative activation energy. This would imply that the hypothetical external agency, conjured up for the purposes of the above analysis, would actually have to *remove* energy from the system to create an instability of this class. Such a wave would clearly exist, however, if $U_\infty > U^*$ in (2.16) when the minus sign is taken; this condition is satisfied for the relatively slow downstream-travelling wave corresponding to DF and GA in figure 2 and to DF in figure 3. For this class of wave any dissipative process would be destabilizing. The physical explanation of the destabilization lies with the slight slowing of the wave in response to the dissipation of its energy (see §2.1).

Class-B waves are a more straightforward case. The external agency must now provide energy to create an instability, so dissipative processes have a stabilizing effect. In this case an irreversible energy transfer from the main stream to the compliant surface would have a destabilizing effect. Miles (1957) and Benjamin (1959, 1963) have shown that the presence of a boundary layer leads to such an irreversible energy transfer (see also §3.1). The boundary layer would have the opposite effect, i.e. stabilizing, on the Class-A waves. It can be seen from (2.16) that $E_A > 0$ when the plus sign is taken and $U^* \neq 0$. These conditions are satisfied for the relatively fast downstream-travelling wave corresponding to FH and GB in figure 2 and BF in figure 3. $E_A > 0$ is also satisfied when $U^* > U_\infty$ and the minus sign is taken in (2.16). These conditions are fulfilled for the upstream-travelling wave corresponding to CD in figure 2 and AD in figure 3.

Class-C instabilities are the only type that can exist in a conservative system. They occur as a coalescence of a Class-A and Class-B instability. From (2.16) it can be seen that the condition for their existence is $U^* = 0$, which corresponds to FG in figure 2 and figure 3. For these instabilities dissipative effects will reduce the growth rate slightly but will not change the stability boundaries.

The simple analysis leading to (2.16) allows one to predict the effects of various irreversible processes on the FISI. For instance, since the relatively slow travelling wave changes from Class B to Class A when U_∞ reaches U_d, it follows that for $U_\infty > U_d$ any dissipative process will generate an instability. Thus, the effects of a viscous fluid substrate or material damping are identical in this respect. On the other hand, for the relatively fast wave instability will set in as soon as there is irreversible energy transfer from the mainstream. It is shown in §3.1 that this occurs when U_∞ reaches c_0. Finally, the analysis suggests that the coexistence of Class-A and Class-B waves brings the possibility of a relatively strong Class-C instability. This point is illustrated in a straightforward way by the present analysis. However, as Benjamin

(1960, 1963) and Landahl (1962) found, the TSI also display the attributes of a Class-A instability; at least they do for most of the unstable region of the (α, Re)-plane (see figure 13 of I, for example). Consequently, a Class-C instability could be expected to occur as a result of a coalescence of the TSI and the fast TWF (Class-B) instability. This type of Class-C instability has been found in I and is further investigated in Carpenter *et al.* (1983) and in Part 3 of the present paper. The energy analysis predicts the existence of such an instability but apparently gives no information on the stability boundaries in this instance.

The type of energy analysis summarized above is presented in a more general form by Benjamin (1963) and other applications are considered in Landahl (1964). Very similar principles were independently developed by Briggs (1964) and others for the treatment of waves in plasmas. Having initially learnt of the concepts through their applications in plasma physics, Cairns (1979) applied them to hydrodynamic instabilities in parallel flows. The Landahl–Benjamin-type analysis has also been applied by Duncan, Waxman & Tulin (1985) to FISI on compliant coatings comprising a homogeneous layer of viscoelastic material. The results are similar to those for Kramer-type coatings.

2.3. *Convective and absolute temporal instabilities*

In the analysis presented above no consideration has been given to the form of the initial disturbance and to how it grows in an unstable flow. Why should such considerations matter? The short answer is that any realistic model of an initial disturbance would give rise to some sort of wavetrain or packet containing a range of frequencies and wavenumbers. Owing to the dispersive nature of the instabilities the development of such waveforms would be characterized by the group velocity rather than the phase velocity.

In the classic experimental investigations of boundary-layer instability by Schubauer & Skramstadt (1948) a vibrating ribbon was used to excite waves; so the initial disturbance was well defined. Gaster (1965*a*, *b*) studied this case theoretically by considering the waveform generated by the ribbon to be a superposition of Fourier eigenmodes of the form

$$\exp\{\mathrm{i}(\alpha' x - \beta' t)\}, \tag{2.17}$$

where α' and β' are both complex. He showed that far from the ribbon the disturbance develops into a spatially growing wave with β' real and equal to the vibrational frequency of the ribbon. This type of instability is quite different from the purely temporal instability represented by (2.1).

The analysis for instabilities of form (2.17) is considerably more involved than for purely temporal instabilities such as (2.1). Consequently, it would be advantageous in the present context if the properties of spatially growing waves could be obtained from an analysis of purely temporal instabilities. Clearly, the actual stability boundaries would be the same for both types of instability. Furthermore, Gaster (1962, 1965*b*) showed that provided the growth rate is small the spatial and temporal eigenvalues are related by

$$\alpha'_{\mathrm{r}} = \alpha, \quad \alpha'_{\mathrm{i}} = -\frac{\alpha c_{\mathrm{i}}}{c_{\mathrm{g}}}, \quad \beta' = \alpha c_{\mathrm{r}}, \tag{2.18}$$

where

$$c_{\mathrm{g}} = \frac{\partial}{\partial \alpha}(\alpha c_{\mathrm{r}}) \tag{2.19}$$

is the group velocity. These relationships seem to be a reasonable approximation for boundary layers on rigid flat plates, so it is tempting to assume that they can be applied to compliant surfaces also. There remains, however, the possibility noted by Gaster (1968) of absolute, or true temporal, instabilities as distinct from the convective†, or spatially growing, waves found in boundary layers on rigid flat plates. For absolute instabilities the group velocity equals zero, so any initial disturbance would grow exponentially with time without being convected from the region of initial excitation. Thus, this type of instability truly grows in time and clearly has a much more profound effect on the flow than the convective type.

The initial disturbances involved in natural transition are due to such sources as free-stream turbulence, acoustic excitation and surface roughness. These are more difficult to represent analytically than the steady sinusoidal input of a vibrating ribbon. However, the pulse input containing, as it does, all frequencies and wave-numbers, could be regarded as reasonably representative of some real disturbances. This case was investigated by Gaster (1968) with free-shear layers in mind, but actually his treatment is fairly general. And very recently Brazier-Smith & Scott (1984) (hereinafter referred to as B-S & S) have investigated the propagation over a compliant surface of waves generated by a pulse input.

The relatively simple case of the stability of a potential flow over a thin plate was studied in depth by B-S & S (see also Atkins 1982). The effects of an elastic foundation were not included (i.e. $K_E = T = 0$ in (2.2)); nor were any dissipative effects considered (i.e. $d = 0$ in (2.2)). Their work is based on techniques developed by Briggs (1964) and Melcher (1981) in plasma physics. In essence, the principle of causality is invoked, i.e. the system is assumed to remain undisturbed until some initial time when an excitation is suddenly applied; the system response after a long lapse of time is then determined.

The root-locus technique used by B-S & S appears to be fairly involved even for the simple test case considered. It would probably be a very difficult undertaking to extend the method to more complex compliant surfaces, with dissipative‡ and boundary-layer effects also included. Consequently, it should be of considerable advantage if the relative simple analysis presented in §2.1 could be used to obtain the main results of the analysis of B-S & S. To show that this is feasible the simple case of the thin plate is investigated and the results of the two approaches compared. The effects of damping are then considered. Finally, the more realistic case of a Kramer-type compliant surface is investigated.

To facilitate a comparison between the results of the present work and that of B-S & S the equivalents of their principal variables in the present notation are given in table 1.

In figure 4 non-dimensional wavenumber is plotted against phase speed and group velocity for two values of C_B^*. The $1/C_A$ vs. $\bar{c}_r$ curves are obtained by evaluating (2.8) when damping is absent and (2.9) in the cases with damping. The group velocity was obtained by applying (2.19) to (2.8) or (2.9). (The non-dimensional group velocity is defined by $\bar{c}_g = c_g/U_\infty$.) The results for $\bar{c}_r$ without damping in figure 4(*a*) are in exact agreement with those presented in figure 9 of B-S & S. This is only to be expected for curves EDF and FH in figure 4(*a*), however, since these curves correspond to neutral stability. In the absence of damping only the branch FG corresponds to an unstable wave.

† The highly apt terms, absolute and convective instability, were borrowed from plasma physics.

‡ Atkins (1982) has incorporated damping in his treatment of the thin plate using the techniques of B-S & S.

Brazier-Smith & Scott (1984)	Present work
K	$1/C_A$
U	$1/(C_B^*)^{\frac{1}{2}}$
Ω	$\bar{c}_r/(C_A(C_B^*)^{\frac{1}{2}})$

TABLE 1. Conversion of variables

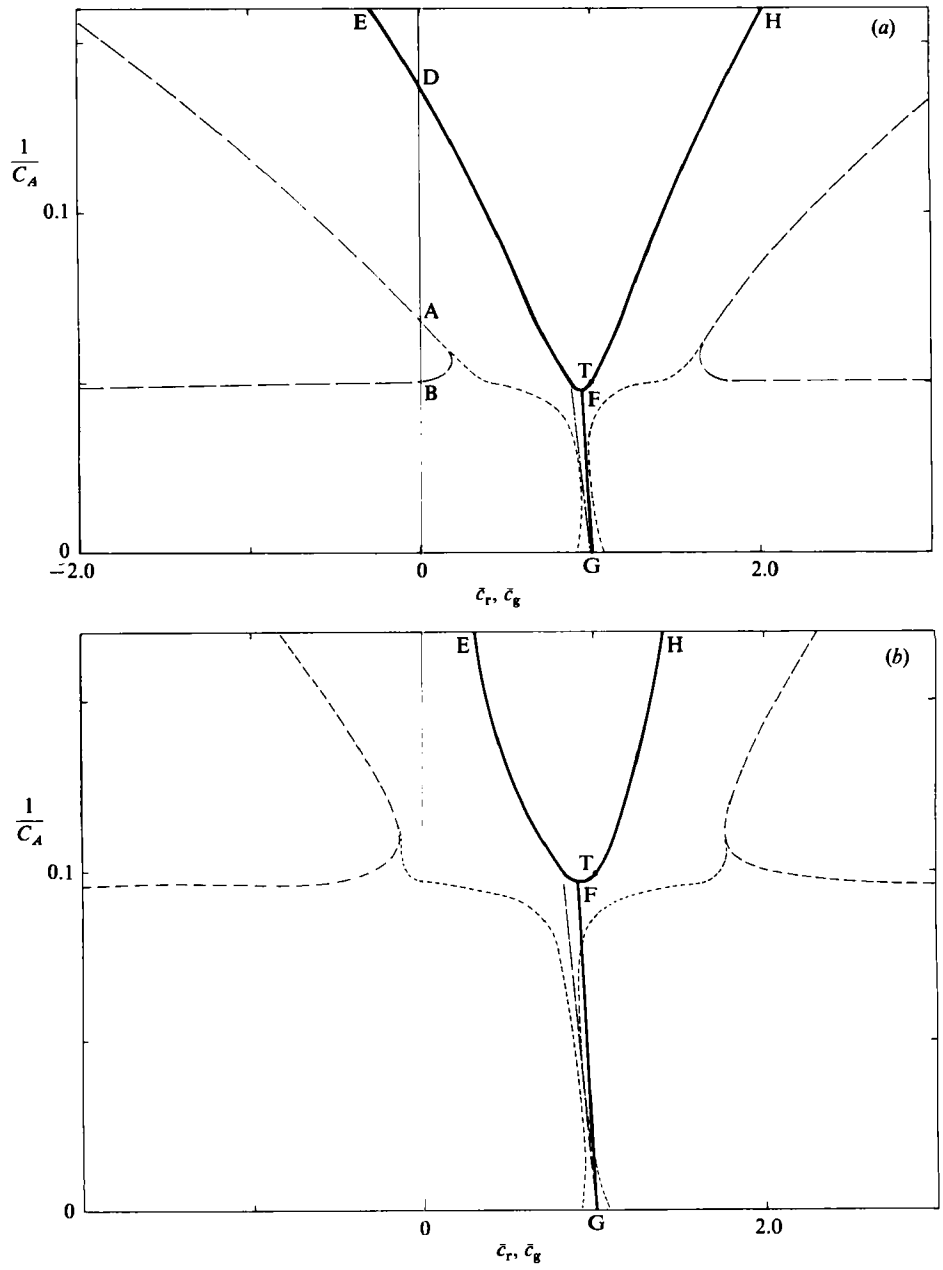

FIGURE 4. Variation of non-dimensional phase and group velocities with non-dimensional wavenumber for a plate with $C_T^* = C_K^* = 0$; (*a*) $C_B^* = 400$, (*b*) 100. ——, $\bar{c}_r$; – – –, $\bar{c}_g$: $C_D^* = 0$; - - - - - - -, $\bar{c}_g$: $C_D^* = 0.01$.

Range of wavenumbers in figure 4(*a*)	Results based on phase speed	
	Brazier-Smith & Scott (1984)	Present methods
Above point D	An outgoing wave upstream. An outgoing wave downstream. Both neutrally stable.	An upstream-travelling wave. A downstream-travelling wave. Both neutrally stable.
Between A and D	Two waves upstream, one incoming and one outgoing. Two outgoing waves downstream. All neutrally stable.	Two downstream-travelling waves. Both neutrally stable.
Between A and F	?	As immediately above.
Between F and G	Upstream – as for region AD. Downstream – one outgoing wave of exponentially growing amplitude.	One downstream-travelling wave of exponentially growing amplitude.

TABLE 2. Comparison of results. In the second column the terms upstream/downstream are used as abbreviations for upstream/downstream of the initial disturbance.

Turning to the curves for group velocity, it will be noted that for non-dimensional wavenumbers lying between A and D in figure 4(*a*) the group velocity is negative while the phase speed is positive. B-S & S referred to this as a region of anomalous propagation.

Since the present methods take no account of the location of the initial disturbance, there is no direct way of determining whether waves are propagating away from or towards the initial input. B-S & S, on the other hand, are able to make such distinctions. A comparison of the results of the two approaches is given in table 2. B-S & S defined the various regions of propagation with reference to values of their variable Ω; hence the uncertainty in the region between points A and F.

In their figure 8 B-S & S plot stability boundaries in terms of $\Omega/U^{\frac{1}{3}}$ vs. U (in their notation). They find that the boundary of the region of anomalous propagation converges on the stability boundary (corresponding to point F in figure 4*a*). At the point where the two boundaries meet they found that the instability changes from being convective to absolute in nature. The stability boundaries given by B-S & S in their figure 8 can be reproduced by the present methods. However, rather than plot the results in the form of $\Omega/U^{\frac{1}{3}}$ vs. U, the corresponding results obtained with the present methods are plotted in figure 5 as non-dimensional wavenumber versus C_B^*. The boundary of the region of anomalous propagation is given by the broken line. For $C_B^* < (C_B^*)_A$ this region extends from D to F (in figure 4) without interruption. $(C_B^*)_A \approx 182$, corresponding to $U = 0.074$, which agrees exactly with B-S & S's critical value U_c marking the onset of absolute instability. Thus, the present method can predict U_c but, without the work of B-S & S, there would be no way of knowing the significance of $(C_B^*)_A$ or U_c, since the results displayed in figure 4(*b*) for $C_B^* < (C_B^*)_A$ (i.e. $U > U_c$) give no indication that the instability has changed in nature.

The effects of damping will now be considered. The instability boundary now moves from F to D in figure 4(*a*). The slower of the two downstream-travelling waves is destabilized by damping as also shown in §§2.1 and 2.2. Now, as one can see from table 2, this wave corresponds either to an incoming wave upstream of the initial impulse input or an outgoing wave travelling downstream. Atkins (1982), using the methods of B-S & S, has shown that it is, in fact, the upstream incoming wave that is destabilized by damping.

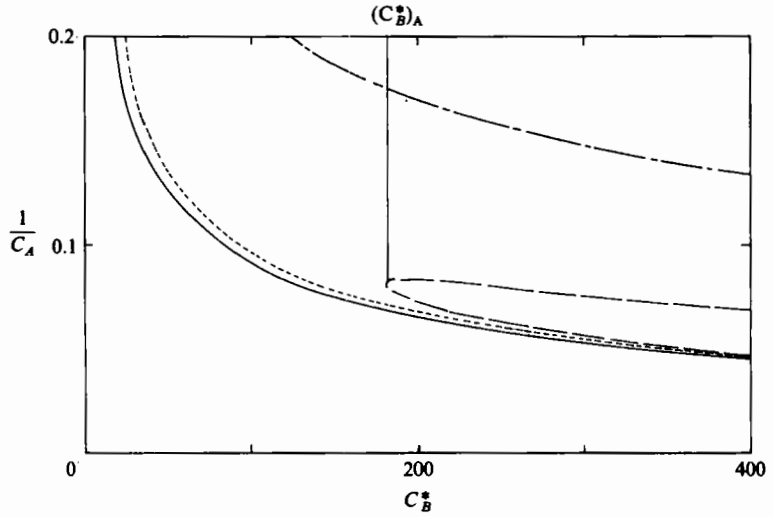

FIGURE 5. Stability boundaries for a plate with $C_T^* = C_K^* = 0$ and no damping. ——, Class-C flutter; — — —, divergence; – – – –, $c_g = 0$; - - - - - - -, $c_r = U_\infty$ (class-B TWF).

Actually, it is very misleading to refer to this destabilized wave as 'incoming'. It may appear to be incoming in terms of phase speed, but when group velocity is considered (see dotted line in figure 4) it is clear that if the development of a waveform were followed it would be dominated by the absolute instability occurring at A in figure 4(*a*). Any initial disturbance containing wavenumbers in the vicinity of point A would tend to spread both upstream and downstream and would grow exponentially with time. Thus the upper portion of the broken line in figure 5 corresponds to absolute instability when damping is present. For $C_B^* < (C_B^*)_A$ the solid line denoting the flutter boundary virtually corresponds to the absolute-instability boundary. The divergence boundary corresponding to point D in figure 4(*a*) marks the onset of convective instability. Thus, when damping is present one would expect the flow field to be dominated completely by an absolute instability at *all* values of C_B^* (i.e. at all flow speeds if B is fixed).

The case of the unsupported thin plate has the merits of simplicity but is rather pathological since it is unstable at all flow speeds. Accordingly, a more practical example of a Kramer-type surface will now be considered.

The case considered in §2.1 and depicted in figure 2 is used again here as an illustrative example. This is partly because it corresponds to the Kramer coating with best performance. In figure 6 non-dimensional wavenumber is plotted against non-dimensional phase speed and group velocity. Only the real part of $\bar{c}$ is plotted, but reference to figure 2 will show that in the absence of damping only the branch FG corresponds to an instability. With damping present DFGA corresponds to an instability. Note that $c_g \approx \frac{1}{2}c_r$ for the Class-C instability corresponding to FG in figures 2 and 6, in contrast with the previous example depicted in figure 4 where $c_g \approx c_r$. Thus it appears that the present example is loosely analogous to gravity waves on the surface of deep water whereas the previous example corresponds more to shallow gravity waves.

It can be seen from figure 6 that the group velocity is zero at points S, R, Q and P when damping is present. Only the point P corresponds to an absolute instability, however. This is because the $\bar{c}_g$ curves passing through R and Q correspond to the

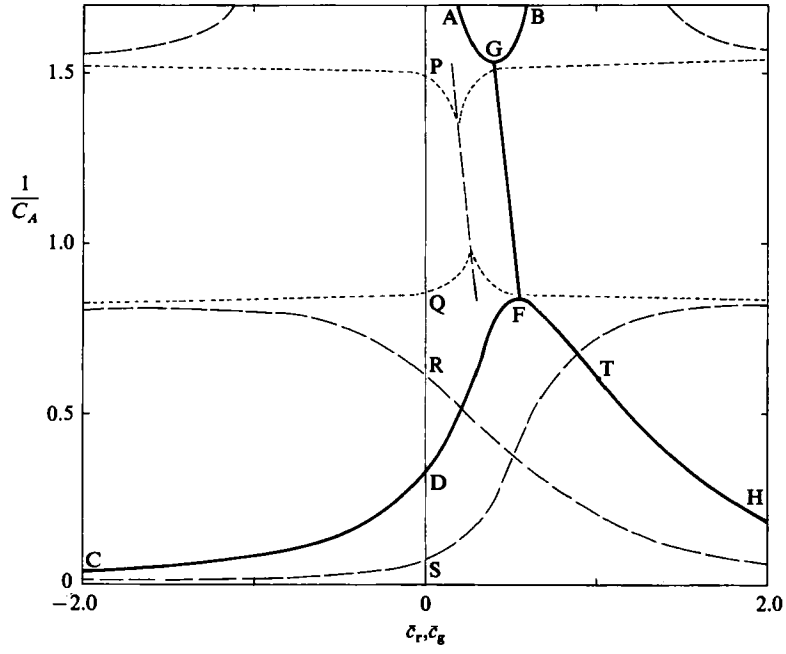

FIGURE 6. Variation of non-dimensional phase and group velocities with non-dimensional wavenumber for Kramer's best coating. $C_B^* = 0.109$, $C_K^* = 0.327$, $C_T^* = 0$. Key as in figure 4. c_g is the same with and without damping where the dotted curve is omitted.

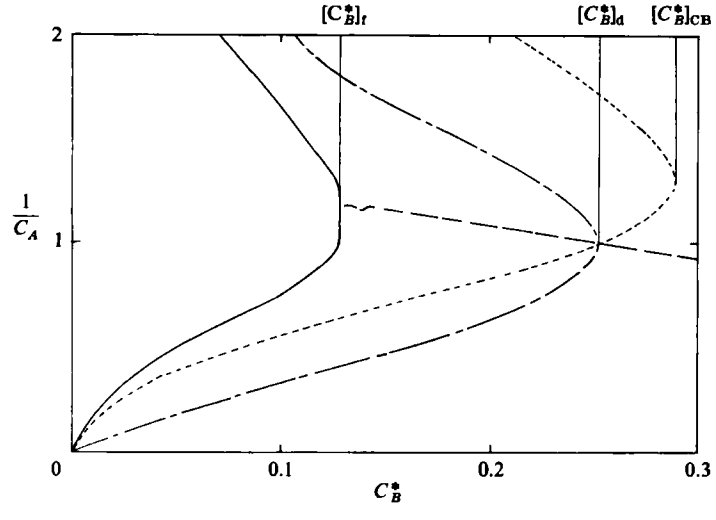

FIGURE 7. Stability boundaries for Kramer's compliant coatings. $C_K^*/C_B^* = 3.0$. ——, class-C flutter; —·—, divergence; – – –, $c_g = 0$; -------, $c_r = U_\infty$ (class-B TWF).

Class-B wave that is stabilized by damping, i.e. to branch FH of the $\bar{c}_r$ curve. Likewise S is located within the wavenumber range below the divergence point D where both waves are Class B, i.e. stabilized by damping.

The stability boundaries for the Kramer coatings are depicted in figure 7 in the form of non-dimensional wavenumber plotted against C_B^*. The $c_g = 0$ curve shown corresponds to the Class-A wave; the corresponding Class-B curves are omitted in

the interest of clarity. The $c_g = 0$ curve corresponding to point P of figure 6 is virtually indistinguishable from the upper portion of the flutter boundary when $C_B^* < (C_B^*)_f$.

It can be concluded from figure 7 that as soon as the divergence speed is reached (corresponding to $(C_B^*)_d$ in figure 7) absolute instability sets in. Thus the Class-A instability corresponding to DF in figures 2, 3 and 6 is not a convective travelling-wave instability but an absolute instability which truly grows with time and which will alter the flow field profoundly. So the term static divergence would not appear inappropriate after all. At this point it may well appear that if FISI occurs it is inevitably an absolute instability. This is not so; as, indeed, the results given in I testify. It will be shown in §3.1 that when boundary-layer effects are taken into account the Class-B wave is destabilized, leading to a conventional convective travelling-wave instability; the stability boundaries for this instability are given by the dotted curves in figures 5 and 7.

3. The effects of irreversible processes on stability

3.1. *Irreversible energy transfer due to the boundary layer*

The shear flow in the boundary layer gives rise to a fluctuating pressure component which is out of phase with the surface motion. This leads to an irreversible transfer of energy from the main stream to the compliant surface – in effect the boundary layer functions as 'negative damping'. Thus, the fast Class-B TWF instability is destabilized by this process and the slow Class-A wave stabilized.

The existence and role of the out-of-phase pressure component appears to have been first explained theoretically for water waves by Miles (1957, 1959*a*, *b*, 1962). His concepts were applied to compliant surfaces by Benjamin (1959, 1963). Benjamin (1963) derived a fairly simple expression for the pressure perturbation δp_e which takes into account the effects of the shear flow in a thin laminar boundary layer. This extremely useful result was obtained by means of an essentially inviscid theory, and takes the form

$$\hat{p}_e(0) = -\rho_e \alpha w_0 \{C_{pr} + iC_{pi}\}(U_\infty - c)^2, \tag{3.1}$$

where

$$C_{pr} = 1 + O(\alpha)$$

and

$$C_{pi} = -\alpha\pi(U_\infty - c_r)^2 \frac{U_c''}{U_c'^3} + O(\alpha^2).$$

The suffix c indicates that the derivatives are to be evaluated at $y = y_c$, where $c_r = U$.

As long as C_{pi} is greater than zero there is, in effect, 'negative' damping which stabilizes the Class-A and destabilizes the Class-B waves according to the energy analysis presented in §2.2. $C_{pi}/(\alpha\delta^*)$, where δ^* is boundary-layer displacement thickness, is plotted against the non-dimensional phase speed $\bar{c}_r$ in figure 8. (These results agree with those plotted in figure 2 of Benjamin (1963) when multiplied by $(1-\bar{c}_r)^2/\bar{c}_r$). It can be seen from figure 8 that C_{pi} is positive when $\bar{c}_r$ lies between 0 and 1.0; it is zero for all other values of $\bar{c}_r$. Accordingly it may be inferred that the Class-B wave is destabilized when $\bar{c}_r$ falls to 1.0 and that the Class-A wave is stabilized from $\bar{c}_r = 0$ upwards, i.e. at the so-called divergence stability boundary. The stability boundary for the Class-B TWF, corresponding to $\bar{c}_r = 1$, is marked by the letter T in figures 2, 3, 4 and 6 and shown by the dotted lines in figures 5 and 7. It is purely coincidental that the critical speeds corresponding to divergence (D) and Class-B TWF (T) are so close in figure 3; and that the points T and F are so near each other in figure 4.

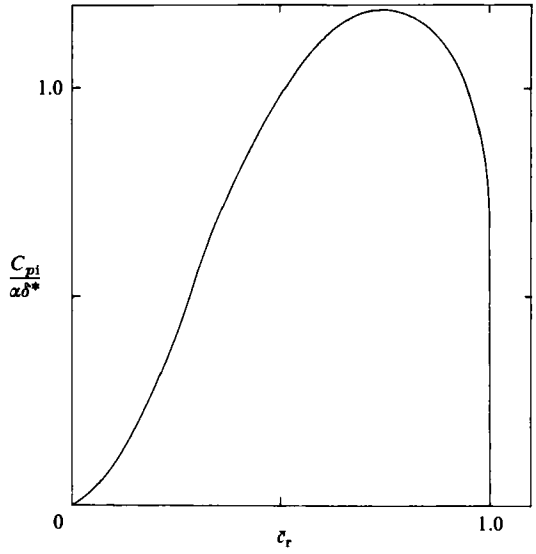

FIGURE 8. The variation of the dimensionless parameter, $C_{pi}/\alpha\delta^*$, with dimensionless phase speed for a laminar boundary layer in zero pressure gradient.

If (3.1) is used to evaluate δp_e in (2.2), (2.5) is replaced by

$$\bar{c}^2-\bar{c}_0^2+C_A(1-\bar{c})^2-\mathrm{i}C_{pi}C_A(1-\bar{c})^2+\frac{\delta p_s}{\rho_m b\alpha^2 U_\infty^2 w}=0. \tag{3.2}$$

For the time being δp_s will be assumed to be equivalently zero. For small values of C_{pi}, i.e. small values of $\alpha\delta^*$, a straightforward small-perturbation analysis of (3.2) can be carried out. The zeroth-order solutions to (3.2), corresponding to $C_{pi}=0$, are given by (2.8). The small change in $\bar{c}$ due to the presence of a thin boundary layer is then given by

$$\Delta\bar{c}=\frac{-\mathrm{i}C_{pi}(1-\bar{c})^2}{2(1-\bar{c})C_A-2\bar{c}}, \tag{3.3}$$

where the symbol $\bar{c}$ on the right-hand side of (3.3) is used for the zeroth-order solutions given by (2.8).

Provided that $U_\infty < U_f$, $\bar{c}$ as given by (2.8) is wholly real and the right-hand side of (3.3) wholly imaginary. Thus it can be seen from (3.3) that instability, which corresponds to $\Delta\bar{c}_i > 0$, will ensue when $(1-\bar{c})C_A-\bar{c}<0$. For Class-A waves it is easily shown, using (2.8), that $(1-\bar{c})C_A-\bar{c}>0$ when $U_\infty < U_f$, showing that the 'negative-damping' effect due to the boundary layer is stabilizing. On the other hand, for Class-B waves $(1-\bar{c})C_A-\bar{c}<0$, implying that the 'negative damping' is destabilizing. Thus, as expected, the small-perturbation analysis confirms the conclusions based on the energy analysis.

It is a relatively simple matter to fit cubic splines to the curve of $C_{pi}/(\alpha\delta^*)$ vs. $\bar{c}_r$ given in figure 8 and to solve (3.2) numerically. In this way the results shown in figure 9 were obtained. The parameters for these results correspond to those for figure 3 with $\delta^*=1$ mm. The results of figure 9 show how the inclusion of the boundary-layer term in (3.2) affects the behaviour of the Class-A and -B waves. Note that, in addition to the effects discussed above, the presence of the boundary layer seems to suppress the coalescence of the Class-A and B waves so that the Class-C flutter instability does

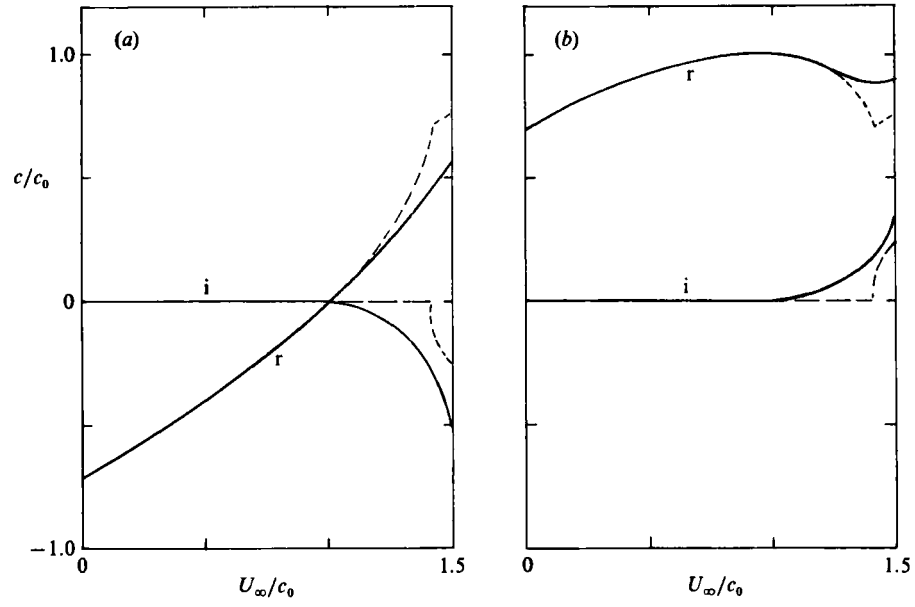

FIGURE 9. Non-dimensional complex wave speed vs. non-dimensional free-stream velocity for a non-dissipative compliant surface without a fluid substrate. $C_A = 1.0$, $\alpha\delta^* = 0.54$. (*a*) Class-A instability; (*b*) class-B instability. r denotes c_r/c_0 and i denotes c_i/c_0. ---, results for potential flow from (2.8), ——, results with boundary layer present obtained by numerical solution of (3.2).

not occur. It can be seen from figure 9(*b*) that beyond $U_\infty/c_0 = 1.0$, c_i grows steadily and that it would not be possible to discern any qualitative change in behaviour when U_f/c_0 is reached. So, effectively, boundary-layer effects ensure that Class-B TWF will occur rather than the Class-C instability.

The results shown in figure 9(*b*) suggest that TWF sets in at $U_\infty = c_0$. This simple result can be readily obtained from (2.8). Since the stability boundary for TWF corresponds to $c = U_\infty$, this value may be substituted into (2.8) (with the plus sign taken on the right-hand side) whence a simple rearrangement gives the result

$$U_\infty = c_0 \tag{3.4}$$

at the stability boundary for TWF.

If (2.6*a*) is substituted for c_0 in (3.4) a quadratic equation for α^2 may be derived, the solution of which gives

$$\alpha^2 = \frac{b\rho_m U_\infty^2 - T \pm \{(b\rho_m U_\infty^2 - T)^2 - 4BK_E\}^{\frac{1}{2}}}{2B}. \tag{3.5}$$

Thus (3.5) gives two positive values of α, α_1 and α_2 say, for the stability boundaries of the TWF. To obtain the neutral curves in the same form as those in I it is necessary to calculate $\bar{\alpha}_{1,2} = \bar{\alpha}_{1,2}\delta^*$, i.e. $\bar{\alpha}_{1,2}\nu_e Re/U_\infty$, where ν_e is the kinematic viscosity of the main-stream fluid and Re is the Reynolds number based on δ^*. In this way the neutral curves presented in figure 10 were obtained. Note that there is good agreement between the curves obtained by the present simple theory, i.e. from (3.5), and those given in I which were obtained by integrating the Orr–Sommerfeld equation numerically. In fact, the present simple theory was required to provide the initial guesses for the eigenvalue search scheme used in I. But it is far more troublesome to compute the TWF than the TSI mode. This is because neutral stability occurs at,

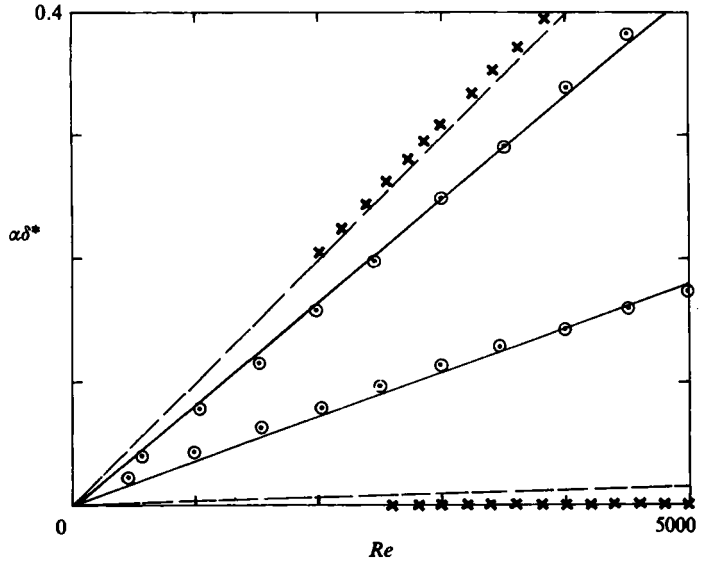

FIGURE 10. Neutral curves for Kramer coating with elastic modulus of 0.5 N/mm^2: ——, without fluid substrate; – – –, inviscid fluid substrate of depth 1 mm and $\rho_s/\rho_e = 0.946$. ○, ×, denote the corresponding results obtained from numerical integration of the Orr-Sommerfeld equation and given in I.

or near, $\bar{c} = 1$. Accordingly, the corresponding eigenvalues are very close to the continuous spectrum and this gives rise to serious computational difficulties. For example, Gaster & Willis (1984) have developed an extremely rapid and convenient method for computing eigenvalues for compliant surfaces which is excellent for the TSI mode but which fails if $\bar{c}$ is greater than about 0.9. In fact, there appears to be no method currently available that can reliably compute eigenvalues close to $\bar{c} = 1$. Consequently, the simple inviscid theory presented above is an important technique for investigating the TWF mode.

Probably the most important results of the present theory are simple formulae for the critical speed and wavenumber. It follows from (3.4) that these formulae can be readily obtained by determining the minimum value of c_0 and the corresponding value of α. Setting to zero the derivative with respect to α of the right-hand side of (2.6a) gives for the critical wave-number

$$\alpha_{cB} = (K_E/B)^{\frac{1}{4}}. \tag{3.6}$$

Substitution of (3.6) for α in (2.6a) gives the minimum value of c_0, and hence from (3.4) the critical speed is given by

$$U_{cB} = \left[\frac{2(BK_E)^{\frac{1}{2}} + T}{b\rho_m}\right]^{\frac{1}{2}}. \tag{3.7}$$

Equations (3.6) and (3.7) were first obtained by Carpenter (1984b).

Note that according to (3.6) the critical wavenumber for a tensioned-membrane surface (i.e. $B = 0$, $T \neq 0$) is infinite. In practice, of course, the flexural rigidity of such surfaces will be small rather than zero and must be taken into account to obtain a realistic estimate of α_{cB}. Furthermore, it would clearly be impossible to investigate the TWF instability by integrating the Orr–Sommerfeld equation numerically if it is assumed that $B = 0$.

The simple results (3.4)–(3.7) only apply to compliant surfaces in the absence of a fluid substrate and damping. When these additional effects are included (3.2), with the appropriate expression for $\delta p_s/w$, must be solved numerically for $\bar{c}$. This will be briefly discussed in §3.2. The case of an inviscid fluid substrate can be easily dealt with by substituting (3.9) (see §3.2) for $\delta p_s/w$ in (3.2) and proceeding in an almost identical fashion to that above. With an inviscid fluid substrate the compliant surface remains non-dissipative and the effect is virtually the same as using a less stiff surface without a fluid substrate, as can be seen from the results plotted in figure 10.

It is well known that the solution (2.8) for a potential flow over a non-dissipative compliant surface gives the wrong stability boundary in the limit as damping tends to zero. Consequently, U_d (given by (2.13)) is generally regarded as the true critical speed rather than U_f (given by (2.14)). The analysis given above makes it clear that the solution (2.8) also gives the wrong stability boundary in the limit as boundary-layer thickness tends to zero. Thus yet another critical speed U_{cB} (given by (3.7)) is obtained. Depending on the properties of the fluid and compliant surface, either U_d or U_{cB} could take the lower value. It is important to note, however, that the corresponding instabilities are quite different from one another.

It is also important to note that although the two types of instability both correspond to eigenmodes† of the coupled Orr–Sommerfeld/compliant-surface equations, they are in fact quite different from one another. TWF is a convective instability, so that (2.1) is a reasonably appropriate representation. Divergence, on the other hand, is an absolute instability, so that (2.1) is probably not an appropriate representation. Certainly, the standing-wave representation adopted in §4 leads to different conclusions with regard to the effect of damping. The critical speed U_{cB} for TWF can be raised by increased damping – in fact the TWF may be completely eliminated in this way – but the critical speed of divergence U_d appears to be unaffected by damping. Transition postponement would not necessarily be ruled out by the existence of TWF but the occurrence of divergence would almost certainly make it unattainable.

3.2. *The effects of viscous and viscoelastic damping*

For real compliant coatings like those of Kramer (1960) irreversible energy losses would occur in two distinct ways. First, losses would occur due to viscous effects in the substrate fluid. Secondly, energy would be dissipated owing to the internal friction of the solid part of the coating which would be made of a viscoelastic elastomeric material. As a convenient shorthand these two effects are referred to here as viscous and viscoelastic damping respectively.

The effects of viscous damping are embodied in the expression for the substrate pressure, δp_s. In I (see equation (3.22)) it was shown that for a viscous fluid substrate

$$\frac{\delta p_s}{w} = \alpha \rho_s c^2 \frac{\beta(\beta+\alpha)\{e^{\beta-\alpha)H} - e^{-(\beta-\alpha)H}\} + \beta(\beta-\alpha)\{e^{(\beta+\alpha)H} - e^{-(\beta+\alpha)H}\}}{8\alpha\beta + (\beta-\alpha)^2\{e^{(\beta+\alpha)H} + e^{-(\beta+\alpha)H}\} - (\beta+\alpha)^2\{e^{(\beta-\alpha)H} + e^{-(\beta-\alpha)H}\}}, \quad (3.8)$$

where H is the depth of the substrate, $\beta^2 = \alpha^2 - i\alpha c/\nu_s$ and ρ_s and ν_s are the density and kinematic viscosity respectively of the substrate fluid. The notation in (3.8) has been changed somewhat from I to fit in with present usage. Two special limiting cases can be derived from (3.8).

† Owing to the close proximity of these eigenmodes to branches of the continuous spectrum, very considerable computational difficulties can be encountered, especially for divergence.

In the limit as $\nu_s \to 0$ (3.8) reduces to

$$\frac{\delta p_s}{w} = \alpha \rho_s c^2 \frac{1+e^{-2\alpha H}}{1-e^{-2\alpha H}}. \tag{3.9}$$

This is the appropriate form for an inviscid fluid substrate, while in the limit $H \to 0$ for fixed ν_s, (3.8) reduces to

$$\frac{\delta p_s}{w} = \frac{12i\alpha^2 \mu_s c}{(\alpha H)^3}, \tag{3.10}$$

where μ_s is the dynamic viscosity of the substrate fluid.

The effects of viscoelastic damping can be taken into account by introducing a complex elastic modulus as explained in I. For present purposes this implies that the flexural rigidity and spring stiffness be multiplied by the complex factor $(1-i\eta)$ where η is the viscoelastic loss factor. In general the loss factor will be different for the flexural rigidity and spring stiffness; but where the same material is used throughout, as in the Kramer coatings, the same value of η may be used in each case. When a single value of η is used, viscoelastic damping may be taken into account by replacing c_0^2 by $c_0^2(1-i\eta)$. For real elastomers η varies with frequency but for simplicity constant values will be assumed in what follows.

With (3.8) substituted for $\delta p_s/w$ and with $\bar{c}_0^2$ replaced by $\bar{c}_0^2(1-i\eta)$, the governing equation (3.2) becomes an even more complicated function of $\bar{c}$. It is relatively easy to solve (3.2) numerically, however, and this is how the results presented below were obtained.

In figure 11 the effects of viscous damping on the behaviour of the Class-A and Class-B TWF instabilities are illustrated. These results correspond to Kramer's best coating with $\alpha = \alpha_d$ and $\delta^* = 1$ mm (i.e. the same as figure 9) and with $\nu_s/\nu_e = 200$. As expected, the viscous damping has a considerable destabilizing effect on the Class-A instability but almost doubles the critical speed of the Class-B TWF.

The stabilizing effect of both kinds of damping on the Class-B TWF is also illustrated in figure 12, where the maximum growth rate, $\bar{\alpha} c_i/c_r$, {where $\bar{\alpha} = \alpha\delta^*$} is plotted against ν_s/ν_e and against η. Note that for $U_\infty = 15$ m/s the results of the present inviscid theory are in close agreement with the results obtained in I by means of the numerical integration of the Orr–Sommerfeld equation. For $U_\infty = 18$ m/s the inviscid theory considerably underestimates the maximum growth rates. This lack of agreement is probably explained by the much larger values of c_i at the higher speed.†

For the Class-A instability the effects of viscous damping and of the 'negative damping' due to the boundary layer act in opposition. The latter effect becomes stronger as the boundary-layer thickness increases. In this way the neutral curves depicted in figure 13 can be explained. For slightly viscous substrates, $\nu_s/\nu_e \leqslant 10$ say, the unstable region in $(\bar{\alpha}, Re)$-space is very small. As ν_s/ν_e rises the unstable region grows until it reaches its fullest extent at $\nu_s/\nu_e \approx 100$. Any further rise in ν_s/ν_e would leave the stability boundaries unchanged. In theory, the neutral curves shown in figure 13 could be found by integrating numerically the Orr–Sommerfeld equation. But, in practice, solutions in the region of $c_r = 0$ are very difficult to obtain. Again, in theory, these Class-A instabilities take the form of travelling waves. But it was shown in §2.3 that they are absolute instabilities, having group velocity equal to zero, so it probably is not sensible to investigate these instabilities as individual eigenmodes.

† Modal interactions between TWF and TSI also occur at 18 m/s.

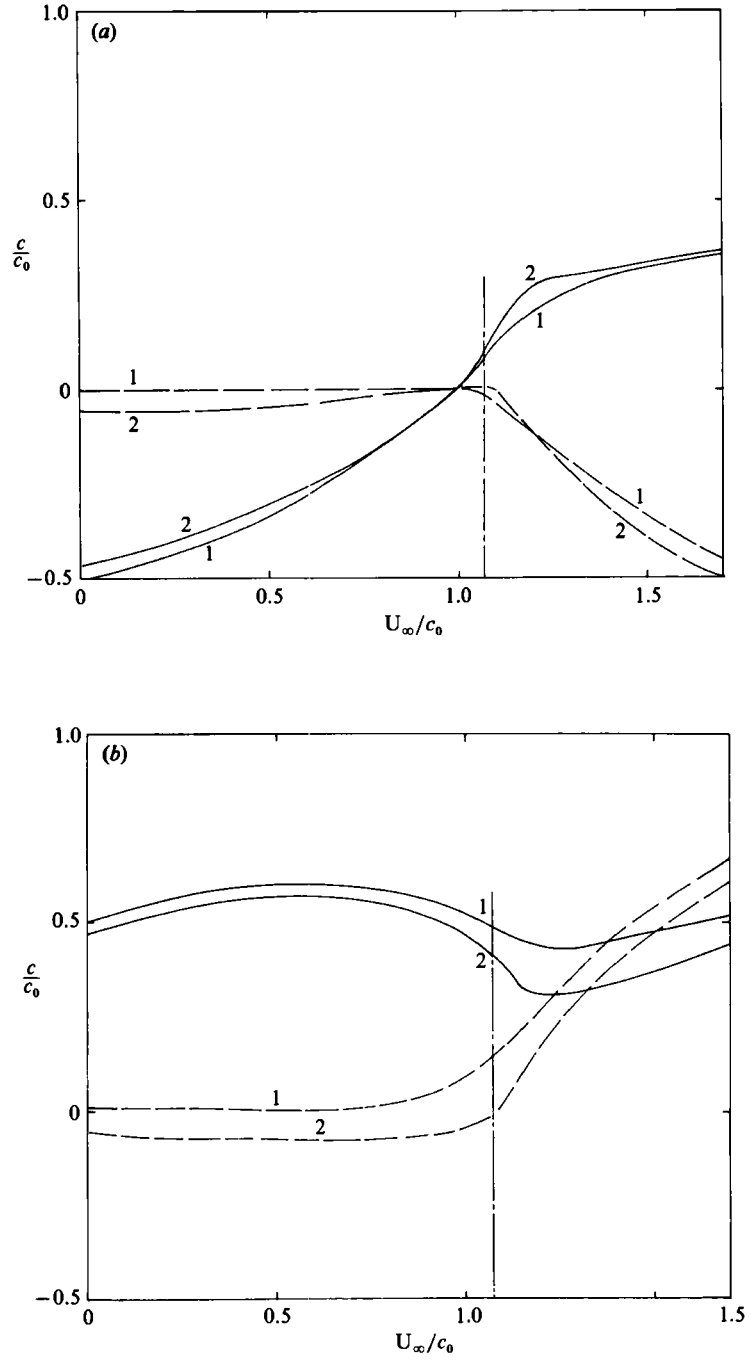

FIGURE 11. Effect of a viscous fluid substrate on travelling-wave flutter for a Kramer coating with elastic modulus of 0.5 N/mm², $\rho_s/\rho_e = 0.946$ and $\alpha\delta^* = 0.54$. ——, c_r/c_0; – – – –, c_i/c_0. 1 denotes $\nu_s/\nu_e = 0$ and 2 $\nu_s/\nu_e = 200$. —·—·—, indicates top operational speed during Kramer's tests. (*a*) Class A, (*b*) Class B.

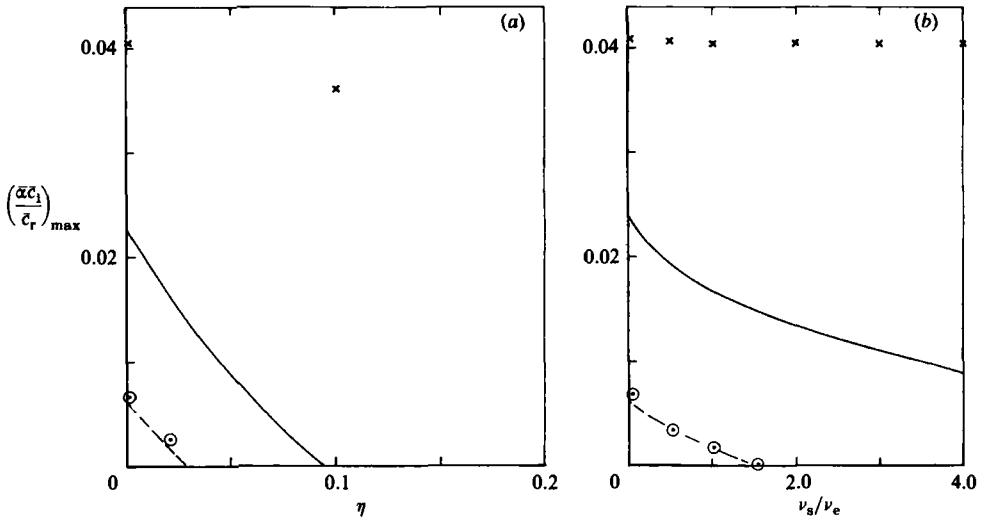

FIGURE 12. Maximum instability growth rate for Class-B TWF plotted against damping factor for Kramer coating with an elastic modulus of 0.5 N/mm^2, $\rho_s/\rho_e = 0.946$ and $H = 1$ mm. For (*a*) $\nu_s/\nu_e = 0$ and for (*b*) $\eta = 0$. ——, $U_\infty = 18$ m/s; – – – – –, 15 m/s: numerical solutions of (3.2). ×, 18 m/s; ○, 15 m/s: numerical solutions of Orr-Sommerfeld equation given in I.

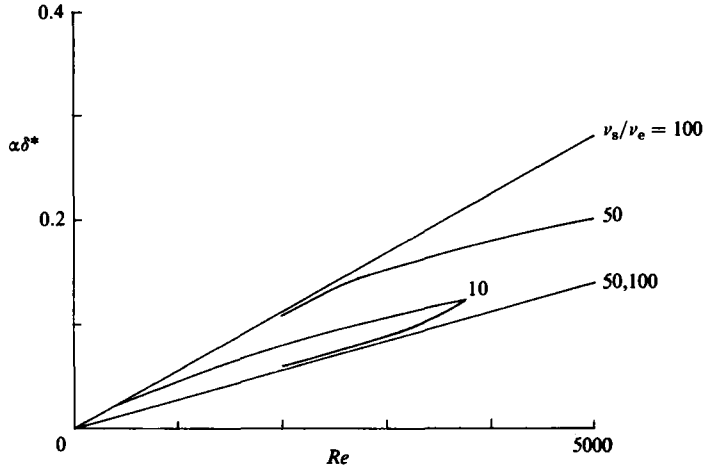

FIGURE 13. Neutral curves for Class-A travelling-wave flutter with various levels of viscous damping. The mechanical properties of the compliant surface are as for figure 12 (*b*).

Some further results, illustrating the effects of viscous damping on the Class-A instability, are presented in Carpenter & Garrad (1982). There it is shown that there is a level of viscous damping which has the maximum destabilizing effect. For the best Kramer coating a value of $\nu_s/\nu_e \approx 400$ yielded the highest instability growth rates. It was also shown in Carpenter & Garrad (1982) that the effects of substrate depth and viscosity are closely inter-related. In fact, as suggested by (3.10), the two effects can be combined by defining a modified viscosity of the form

$$\mu_r = \frac{\mu_s}{(\alpha H)^3}. \tag{3.11}$$

This implies that two coatings with the same value of μ_r would have very similar levels of viscous damping. This has been established by Carpenter & Garrad (1982) for the Class-A instability, but presumably would also hold for the TSI and Class-B TWF.

It would also be possible to investigate the effects of viscoelastic damping on the Class-A instability. It is important to note, however, that the sign of the imaginary part of the elastic modulus depends on the sign of αc_r – as demonstrated in I. Therefore, when considering the upstream-propagating wave which occurs at free-stream speeds below U_d, the factor $(1-i\eta)$ must be replaced by $(1+i\eta)$. Real elastomers tend to exhibit low levels of damping at low frequencies. Consequently, in practice η will be very small in the vicinity of the stability boundary for Class-A instabilities where frequency (i.e. αc_r) is zero. Thus it is thought that viscoelastic damping will have little effect on the Class-A instabilities.

4. Static divergence

A fairly complete picture of the flow-induced instabilities of a compliant surface has apparently emerged from the theory described in the preceding sections. Focusing on the Class-A instability, one finds that it takes the form of a slow downstream-travelling wave and that damping is essential for its existence. In fact, it would appear from figure 13 that a level of damping equivalent to a viscous fluid substrate about ten times more viscous than water would be required for the unstable region in $(\bar{\alpha}, Re)$-space to reach a significant size. On the other hand, it was shown in §2.3 that the Class-A instability is absolute and, consequently, it should have a far more profound effect on the flow than the purely convective Class-B TWF.

The conclusions reached above concerning the essential role played by the damping and the travelling-wave nature of the Class-A instability run counter to known results for the hydroelastic stability of flexible surfaces having finite length (see Dugundji, Dowell & Perkin 1963; Weaver & Unny 1970; Dowell 1975; Kornecki, Dowell & O'Brien 1976; and Garrad & Carpenter 1982*b*). For finite flexible surfaces both static divergence and standing-wave flutter instabilities can occur in general. Moreover, damping is not necessary for either type of instability. In view of these results one is prompted to speculate on whether the results obtained using the finite-length theory in the limit as $\alpha L \to \infty$ (where L is the length of the compliant surface) will agree with those obtained using the theory in the preceding sections. This point is investigated in the next paragraph.

For a compliant surface of finite length L an instability of general standing-wave form is assumed, i.e.

$$w(x,t) = \exp(i\omega t) \sum_{n=1}^{\infty} LA_n \sin\left(\frac{n\pi x}{L}\right), \tag{4.1}$$

where $\omega = \omega_r + i\omega_i$ is the complex frequency.

In Garrad & Carpenter (1982*b*) the main-stream pressure was obtained by means of thin-aerofoil theory whereby the main-stream flow was modelled by a source distribution. Galerkin's method was then followed to obtain a matrix equation for the coefficients A_n which, in the absence of a fluid substrate, takes the form

$$B_{mn} A_n = 0 \quad (m, n = 1, \ldots, \infty), \tag{4.2}$$

where the matrix coefficients are given by:

$$B_{mn} = \{m^4 \bar{C}_B + \bar{C}_K + i\bar{C}_D \Omega - \Omega^2\} \delta_{mn} - (\bar{C}_M/\pi)\{4i\Omega Fr I_{1nm} + 2nFr^2 I_{2nm} - \pi\Omega^2 I_{3nm}\} \tag{4.3}$$

The non-dimensional coefficients are defined as follows:

$$\overline{C}_B = \frac{\pi^2 B}{b\rho_m g L^3}, \quad \overline{C}_K = \frac{K_E L}{\pi^2 b\rho_m g}, \quad \overline{C}_D = \frac{\mathrm{d}L^{\frac{1}{2}}}{b\rho_m g^{\frac{1}{2}}}, \quad \overline{C}_M = \frac{\rho_e L}{b\rho_m}. \tag{4.4}$$

The non-dimensional complex frequency and mainstream velocity are defined respectively as

$$\Omega = \frac{\omega L^{\frac{1}{2}}}{\pi g^{\frac{1}{2}}}, \quad Fr = \frac{U_\infty}{(gL)^{\frac{1}{2}}}. \tag{4.5}$$

The latter is in the form of a Froude number, hence the notation. I_{1nm}, I_{2nm} and I_{3nm} are integrals which are defined as

$$\begin{aligned} I_{1nm} &= \int_0^1 \int_0^1 \frac{\sin(n\pi\xi)\sin(m\pi\zeta)}{\zeta-\xi}\,\mathrm{d}\xi\,\mathrm{d}\zeta, \\ I_{2nm} &= \int_0^1 \int_0^1 \frac{\cos(n\pi\xi)\sin(m\pi\zeta)}{\zeta-\xi}\,\mathrm{d}\xi\,\mathrm{d}\zeta, \\ I_{3nm} &= \frac{2}{n\pi}\left[\{1+(-1)^{n+m}\}\int_0^1 \ln(\xi)\sin(m\pi\xi)\,\mathrm{d}\xi - I_{2nm}\right]. \end{aligned} \tag{4.6}$$

The limit $\alpha L \to \infty$ is equivalent to n and $m \to \infty$. It can be shown† that as n and m tend to infinity $I_{1nm} = I_{3nm} = 0$ and $I_{2nm} = \frac{1}{2}\pi$ if $n = m$, $I_{2nm} = I_{3nm} = 0$ if $n \neq m$, $I_{1nm} = 1/(n-m)$ if n is even and m odd or vice versa, and $I_{1nm} = 0$ if n and m are either both odd or both even.

The characteristic equation for determining the non-dimensional complex frequency Ω is obtained from (4.2) by setting the determinant of B_{mn} equal to zero, i.e.

$$\det(B_{mn}) = 0. \tag{4.7}$$

If a single-mode disturbance is considered (4.7) reduces to

$$B_{nn} = 0. \tag{4.8}$$

Substitution in (4.3) of the values assumed by I_{1nm} etc. in the limit as $n \to \infty$ and taking $\overline{C}_D = 0$ gives the following form for (4.8):

$$n^4\overline{C}_B + \overline{C}_K - \Omega^2 - \frac{n}{\pi}\overline{C}_M Fr^2 = 0. \tag{4.9}$$

Since the other three terms in (4.9) are real Ω^2 must also be real, so Ω must either be real or purely imaginary. Thus, only a divergence-type instability is possible for a single-mode disturbance. The critical value of velocity (or, equivalently, Fr) is obtained from (4.9) by setting $\Omega = 0$, giving

$$Fr_{\mathrm{d}} = \left[\frac{\pi(n^4\overline{C}_B + \overline{C}_K)}{n\overline{C}_M}\right]^{\frac{1}{2}}. \tag{4.10}$$

The minimum value of Fr_{d} corresponds to a mode number of

$$n_{\mathrm{c}} = \left(\frac{\overline{C}_K}{3\overline{C}_B}\right)^{\frac{1}{4}} = \frac{L}{\pi}\left(\frac{K_E}{3B}\right)^{\frac{1}{4}}. \tag{4.11}$$

Equations (4.10) and (4.11) were previously derived by Garrad & Carpenter (1982*b*) and have recently been generalized to oblique waveforms on orthotropic panels by

† The treatment of the singularities involved in I_{2nm} is described in Garrad & Carpenter (1982*a*).

Carpenter (1984*c*). The mode number n_c of the most unstable mode given by (4.11) agrees exactly with (2.12) when $\pi n/L$ is identified with α. The critical velocity obtained by substituting (4.11) into (4.10) also agrees exactly with the result (2.13) of the simpler infinite-length theory.

As shown above, the theory for standing waveforms of finite length gives the same results for the critical wavelength and velocity in the limit as $n \to \infty$ as the infinite-length theory developed in §§2 and 3. But, whereas a substantial level of damping is required to produce the Class-A TWF instability, the divergence instability occurs in the absence of damping. In fact, Carpenter & Garrad (1982) have shown that the introduction of damping reduces the growth rate of divergence.

How should the divergence instability be classified according to the energy analysis described in §2.2? The fact that its occurrence does not require any form of irreversible energy transfer suggests that it is a Class-C instability. A closer inspection reveals that matters are not quite that straightforward. For free-stream speeds below U_d there are two neutrally stable standing waves of the form

$$w = w_0 \, e^{\pm i\omega_r t} \sin(\alpha x). \tag{4.12}$$

A straightforward analysis shows that for both these waves the activation energy is positive, so the waves are Class B. This corresponds exactly to the travelling-wave analysis described in §2 in that for $U_\infty < U_d$ the travelling waves corresponding to AD and BF in figure 3 were also found to be Class B.

The classification of the standing wave for $U_\infty > U_d$ depends on what is assumed about the final state of the wave. After the divergence speed has been exceeded the wave changes form to

$$w = w_0 \, e^{\omega_r t} \sin(\alpha x), \tag{4.13}$$

so if one assumes a non-growing final state, as in §2.2, then this implies that $\omega_r = 0$ and it can be readily shown that $E_A = 0$, i.e. the wave is Class C. However, it is somewhat illogical to assume a non-growing final state when the stability analysis indicates that $\omega_r > 0$ when $U_\infty > U_d$. Accordingly, the energy analysis was repeated assuming a growing final state and the rate of change of activation energy with time was found to be

$$\frac{dE_A}{dt} \sim -\tfrac{1}{2}\rho_e \omega_r^3 e^{2\omega_r t}. \tag{4.14}$$

Since ω_r is small dE_A/dt is clearly small, but equally clearly it is negative, indicating a Class-A instability. This, of course, corresponds to the situation found with the travelling-wave analysis when a non-growing final state is assumed.

The situation now appears rather paradoxical. On the one hand the stability analysis shows quite clearly that damping is not required to produce single-mode divergence. But on the other hand the energy analysis appears to show that the divergence instability is a Class-A wave which implies that damping is required for the instability to occur. A completely satisfactory resolution of this apparent paradox has eluded us thus far, but a possible explanation is set out below.

The fact that dE_A/dt is negative for a divergence instability could be interpreted as meaning that a small surplus of energy is being generated. The question then becomes: What happens to this energy surplus? When considering this question it should be noted that for the Galerkin-type analysis of the stability of finite compliant surfaces it is only an approximation to consider the modes individually. Strictly an infinite number of modes should be considered simultaneously. Suppose that the mode considered in the single-mode analysis is the most unstable, i.e. the one with the lowest critical velocity. As soon as U_∞ exceeds this critical velocity the possibility exists of

adjacent modes being excited by energy transfer from the most unstable mode. If this happens one would expect the critical velocity of the adjacent modes to be slightly lower than predicted by the single-mode analysis. In fact, this lowering of the critical velocity was found in the triple-mode analysis presented by Garrad & Carpenter (1982*b*). Since the energy transfer to adjacent modes was ignored in the energy analysis given above, it provides a possible explanation to the question posed above concerning the apparent energy surplus.

When multiple-mode, rather than single-mode, standing-wave disturbances are considered it can be shown that two modes may coalesce, thereby giving rise to a conventional Class-C instability. This type of instability is known as standing-wave flutter and takes the form of an oscillating standing wave. Let us consider a waveform (4.1) consisting of an indefinite number of modes clustered about the most unstable mode of mode-number n_c. Since $n_c \gg 1$, it can be assumed to a good approximation that

$$B_{n_c-l,n_c-l} = B_{n_c,n_c}$$

provided that l is $O(1)$. When $m = n$, it follows from (4.3) and the asymptotic forms for I_{1nm} etc., that

$$B_{mn} = -\frac{1}{n-m}B^* \quad \text{when } n-m \text{ is odd},$$

$$= 0 \qquad\qquad \text{when } n-m \text{ is even},$$

where $B^* = 4\mathrm{i}\,\overline{C}_M\,\Omega Fr/\pi$, giving

$$\begin{vmatrix} \cdot & \cdot & \cdot & \cdot & \cdot & \cdot & \cdot \\ \cdot & B_{nn} & B^* & 0 & \frac{1}{3}B^* & 0 & \cdot \\ \cdot & -B^* & B_{nn} & B^* & 0 & \frac{1}{3}B^* & \cdot \\ \cdot & 0 & -B^* & B_{nn} & B^* & 0 & \cdot \\ \cdot & -\frac{1}{3}B^* & 0 & -B^* & B_{nn} & B^* & \cdot \\ \cdot & 0 & -\frac{1}{3}B^* & 0 & -B^* & B_{nn} & \cdot \\ \cdot & \cdot & \cdot & \cdot & \cdot & \cdot & \cdot \end{vmatrix} = 0 \qquad (4.15)$$

For simplicity suffix n is used for suffix n_c in (4.15). For odd numbers of modes it appears that (4.15) can be expanded and subsequently factorized to give equations of forms equivalent to

$$B_{nn}(B_{nn}^2 + \lambda B^{*2}) = 0, \qquad (4.16)$$

where $\lambda = 2$ for three modes and $\frac{16}{9}$ for five modes.

Thus one factor of (4.16) leads again to (4.8), and a single-mode divergence with the same critical speed as before is obtained. The other factor leads to a quadratic in Ω^2. The condition for $\Omega^2 = 0$ leads again to (4.8) but the condition for complex Ω^2 (implying a Class-C instability) leads to a critical velocity given by

$$Fr_f = Fr_d\left\{1 - \lambda\frac{4\overline{C}_M}{n\pi^3(n-m)^2}\right\}^{-\frac{1}{2}}. \qquad (4.17)$$

For Kramer's coatings (4.17) gives the following critical velocities for standing-wave flutter:

$$\left.\begin{aligned} U_f &= 3.3U_d \quad (3 \text{ modes}), \\ U_f &= 1.9U_d \quad (5 \text{ modes}). \end{aligned}\right\} \qquad (4.18)$$

In practice, a small disturbance will contain a large number of modes. Consequently, for application to real surfaces it would be unwise to place too much reliance on the results given in (4.18). It does, however, appear that the critical velocity for flutter is much higher than that for divergence. Accordingly, one would not expect to observe standing-wave flutter on Kramer-type coatings.

A certain amount of experimental work has been carried out on the flow-induced surface instabilities, mostly divergent in character, occurring on a variety of compliant surfaces. This work is briefly reviewed below.

Wrinkles and pulsations of Kramer coatings were reported by Puryear (1962), Ritter & Messum (1964), Ritter & Porteous (1965) and Nisewanger (1964). Puryear presented a photograph showing the wrinkles and gave a value for the critical velocity. Garrad & Carpenter (1982*b*) showed that the results of the present theory for critical wavelength and speed are in good agreement with the empirical observations of Puryear. Similar types of hydroelastic instability have also been observed on dolphins, notably by Essapian (1955). Some scientists, e.g. Hertel (1963), have proposed that this skin folding is actively controlled by the dolphin in order to achieve favourable hydrodynamic effects. However, in view of the fact that Aleev (1973, 1977) has observed a very similar phenomenon on young female human subjects, it would appear fairly certainly to be a divergence type of hydroelastic instability.

It appears that no detailed experimental investigation of the flow-induced surface instabilities on Kramer-type surfaces has been undertaken. Some very careful and detailed studies have been carried out on related surfaces though; for example Dugundji *et al.* (1963), MacMichael, Klebanoff & Mease (1980), Hansen & Hunston (1974, 1976, 1983), Hansen *et al.* (1980*a*, *b*), Gad-el-Hak, Blackwelder & Riley (1984) and Gad-el-Hak (1985, 1986*a*). Dugundji *et al.* studied the aeroelastic behaviour of an aluminium panel supported on springs. They observed mild divergence-type instability ($n_c \approx 7$–11) which had travelling-wave flutter superimposed on it when the flow speed reached a sufficiently high level. MacMichael *et al.* (1980) made detailed measurements of the response of a tensioned-membrane-type compliant surface to turbulent air flow. They observed both Class-B travelling-wave disturbances and static divergence. Homogeneous, isotropic compliant surfaces in the form of plastisol slabs have been fairly extensively studied by Hansen & Hunston (1974, 1976, 1983) and Hansen *et al.* (1980*a*, *b*). Very recently Gad-el-Hak *et al.* (1984) have presented some impressive results of a detailed investigation of the response of such surfaces to a turbulent water flow. They observed what they termed 'static divergence' but, in fact, these instabilities were slowly travelling waves with phase speed increasing with flow speed above the critical speed, typically $c_r \approx 0.05U_\infty$. These instabilities only appeared when the boundary layer was turbulent. Hansen & Hunston (1976, 1983) have observed similar hydroelastic instabilities in compliant coatings on spinning disks. In this case, however, the instabilities were observed in both the laminar and turbulent regimes. The propagation speed of the waves was negligible in both regimes but the instability had a strikingly different appearance in the two regimes. In particular, the wavelength was much longer when the flow was laminar. Hansen & Hunston also found that their simple theoretical predictions of the critical speed for a divergence-type instability agreed well with the observed behaviour in the laminar regime.

Very recently Gad-el-Hak (1985, 1986*a*) has presented the results of an experimental study of the waves generated by turbulent water flow over homogeneous, isotropic compliant surfaces made of common, household gelatin. The significance of gelatin lies in its extremely low viscoelastic damping. Thus, it is very nearly a truly elastic

solid. Gad-el-Hak found that the waves on the gelatin (i.e. elastic) surfaces were quite different from those on the plastisol (i.e. viscoelastic) surfaces. The waves on the elastic surfaces had phase speeds of between 25 % and 50 % of the free-stream speed, compared with 0.5 %–5 % for the viscoelastic surfaces. The waves on the elastic surfaces also had smaller wavelength and amplitude as compared with those on the viscoelastic surfaces.

Gad-el-Hak (1985) has also carried out some experiments on silicone-rubber surfaces. In this case, by varying the composition of the silicone rubber it is possible to make surfaces with levels of viscoelastic damping that vary from very low to moderate. For low-damping surfaces Gad-el-Hak found that the fast (elastic) waves were generated. But when the damping exceeded a critical threshold the divergence-type, slow (viscoelastic) waves took over.

These recent results of Gad-el-Hak strongly suggest that damping is essential for the generation of a divergence-type instability. There is, however, an alternative interpretation of these experimental observations. Fraser & Carpenter (1985) have shown that in the absence of damping the critical speeds for TWF and divergence for laminar flow over homogeneous, elastic compliant surfaces are given approximately by

$$U_{\mathrm{CB}} = C_{\mathrm{s}}, \quad U_{\mathrm{d}} = C_{\mathrm{T}}\left\{2\frac{\rho_m}{\rho_{\mathrm{e}}}\left(1-\frac{C_{\mathrm{T}}^2}{C_{\mathrm{L}}^2}\right)\right\}^{\frac{1}{2}}, \tag{4.19}$$

where C_{s} is the velocity of free surface waves on the compliant surface and C_{T} and C_{L} are respectively the propagation speeds of shear and longitudinal waves in the solid. When $C_{\mathrm{T}}/C_{\mathrm{L}} = 0$ the above result for U_{d} agrees with that derived by Hansen & Hunston (1974). For elastomers like plastisol and silicone rubber $C_{\mathrm{T}}/C_{\mathrm{L}}$ is very small and $\rho_{\mathrm{m}}/\rho_{\mathrm{e}} \approx 1.0$ so that $U_{\mathrm{d}} \approx \sqrt{3}\,C_{\mathrm{T}}$ whereas $C_{\mathrm{s}} \approx 0.95 C_{\mathrm{T}}$. Thus it can be seen that in the absence of damping TWF always has a lower critical speed than divergence for homogeneous, isotropic compliant surfaces. But viscoelastic damping has a stabilizing effect on the TWF, so that as the level of damping rises U_{CB} also increases. On the other hand the divergence speed is left unchanged by the inclusion of damping. Thus, as damping is increased a level will be reached at which $U_{\mathrm{CB}} = U_{\mathrm{d}}$ and divergence will take over from TWF.

It has been pointed out above that there are substantial differences between the results for a divergence-type instability obtained with a travelling-wave analysis and those obtained by means of a standing-wave analysis. First there is the question of whether the instability manifests itself as a travelling wave or as truly static divergence. Experimental evidence indicates that the travelling-wave form of divergence occurs on some types of compliant surface in turbulent flow but it is still not known whether this form of the instability can occur for laminar flow over a Kramer-type compliant surface. If the standing-wave analysis had indicated the occurrence of standing-wave flutter rather than divergence then there would be no real differences between the forms used in the two theoretical approaches. The indications appear to be that in the case of laminar flow the critical speed for standing-wave flutter is considerably higher than that for divergence in the case of Kramer-type compliant surfaces. However, Garrad & Carpenter (1982*b*) have shown that standing-wave flutter will take over from divergence if the mainstream changes from laminar to turbulent. Secondly, there is the question that the damping is essential for the occurrence of divergence. The travelling-wave analysis clearly indicates that damping is essential whereas the standing-wave analysis equally clearly indicates that divergence can occur in the absence of damping.

It cannot be claimed that the differences between the two approaches have been

completely satisfactorily explained or resolved in the present paper. Perhaps, though, these differences are not so significant in practice as might appear at first sight. The point is that it has been shown by the travelling-wave analysis that divergence is an absolute instability and this is certainly consistent with experimental observation. The standing-wave analysis implicitly assumes an absolute instability. For such an instability the distinction between travelling and standing waves tends to lose its significance. Moreover, such concepts as stability boundaries in $(\bar{\alpha}, Re)$-space (see figure 13) and instability growth rate are now all but irrelevant. All that matters for an absolute instability is whether or not it exists. Even if its growth rate is very small, and the unstable wavenumbers are confined to a diagonal line in the $(\bar{\alpha}, Re)$-plot in figure 13, the instability will still develop and given time will eventually dominate the flow field, thereby destroying any potential transition-delaying characteristic of the surface.

5. Conclusions

The flow-induced surface instabilities of Kramer-type compliant surfaces have been investigated by means of a variety of theoretical approaches. The results should be applicable to any compliant surface which consists of a thin elastic plate, with or without applied longitudinal tension, supported on a springy elastic foundation, with or without a viscous fluid substrate; material damping is also taken into account through the viscoelastic properties of the solid constituents of the coating. Four possible instability modes have been identified and investigated, namely Tollmien–Schlichting instability (see I), (Class B) travelling-wave flutter, static divergence, and a combined instability formed by the interaction and coalescence of the Tollmien–Schlichting and travelling-wave-flutter instabilities (see I and Carpenter *et al.* 1983). Three additional instability modes have been identified theoretically, namely Class-A travelling-wave flutter, Class-C travelling-wave flutter and standing-wave flutter. For a variety of reasons, however, these additional instabilities are not considered likely to occur in practice. A summary of the main characteristics of the various instabilities is given in table 3.

In table 4 a summary of results is presented for the instabilities on the original Kramer (1960) coatings. The top operational speed during Kramer's tests was 18 m/s, so it can be concluded that probably only his softest coating (D) suffered from static divergence. This is probably the explanation for its poor performance, its drag being virtually the same as for the rigid reference surface at the top speed (see figure 3 of I). Coatings C and D should have experienced travelling-wave flutter, but as shown in I this instability can be reduced or eliminated by damping (i.e. by the introduction of a viscous fluid substrate). It was shown in I that at the top speed of 18 m/s this procedure was frustrated because the introduction of damping brought about the occurrence of modal interaction between the Tollmien–Schlichting and travelling-wave-flutter instabilities. There are grounds,† however, for believing that this interaction would be unlikely to occur on the actual Kramer coating. In the absence of modal interaction it was shown in I that Coating C had a reasonable performance with respect to transition delay. On the other hand, the stiffest coating (B) has a much less stabilizing effect on the Tollmien–Schlichting instabilities. Therefore, despite the absence of any flow-induced surface instabilities in this case, the transition delay achievable with this coating would be much less than for coating C. Hence the drag

† For example, Kramer's model was axisymmetric, so there may well have been significant three-dimensional effects which have been ignored in the present analysis.

Instability	Class	Type	Effect of a reduction in coating property: Stiffness $b\rho_m c_0^2$	Effect of a reduction in coating property: Mass $b\rho_m$	Effect of damping	Effect of an increase in boundary-layer thickness
TSI	A	C	CV U	CV U	CV U	.
			A−	A+	A+	A+
			GR−	GR+	GR+	GR+
Class-A TWF	A	A	CV−	CV U	CV U	CV U
			A (see (2.12))	A U	A+	A−
			GR+	GR U	GR+	GR−
Class-B TWF	B	C	CV−	CV+	CV+	CV−
			A (see (3.6))	A−	A−	A+
			GR+	GR−	GR−	GR+
Divergence	C?	A	CV−	CV U	CV U	CV U
			GR+		GR−	GR U
Combined TSI/TWF	C	C	.	.	Promoted by damping	A+ GR+

TABLE 3. A summary of the main characteristics of the various instabilities. In column 3 C and A denote convective and absolute instabilities respectively. In columns 4–7, CV denotes critical velocity, A area of instability region in $(\bar{\alpha}, Re)$-plane, GR instability growth rate; U, +, − denote no change, increase and decrease respectively.

Coating designation in Kramer (1960)	Elastic modulus (E/mm^2)	Critical velocity (m/s)		Critical wavelength (mm)			
		TWF	Div	TWF	Div	TSI	Combined TSI/TWF
B	1.04	22.3	24.6	8.8	11.6	—	—
C	0.52	15.8	17.4	8.8	11.6	20	3
D	0.40	13.9	15.3	8.8	11.6	—	—

TABLE 4. Summary of results for instabilities on original Kramer (1960) coatings

for coating B should be higher than for coating C, as is found in figure 3 of I. Thus Kramer's experimental observations are more or less consistent with the predictions of linear hydrodynamic stability theory. As could no doubt have been anticipated, however, the theoretical studies have by no means conclusively demonstrated that Kramer's coatings are capable of achieving substantial delays in transition to turbulent flow.

The authors would like to thank Dr M. Purshouse for introducing them to the work of Aleev. They also wish to acknowledge the valuable information and advice provided by Dr M. Gaster and Mr G. J. K. Willis of British Maritime Technology during many helpful discussions. The work described above is part of a research programme at Exeter which is being carried out with the support of Procurement Executive, Ministry of Defence; it was started when one of the authors (Garrad) was in receipt of an SERC studentship.

REFERENCES

ALEEV, YU. G. 1973 Dolphins and women. *Khimia i zhizn* **9**, 8–10 (in Russian).

ALEEV, YU. G. 1977 *Nekton*. The Hague: Junk.

ATKINS, D. J. 1982 The effect of uniform flow on the dynamics and acoustics of force-excited infinite plates. *Admiralty Marine Technology Establishment, Teddington, England, Tech. Memo*, AMTE (N) TM 82087.

BENJAMIN, T. B. 1959 Shearing flow over a wavy boundary. *J. Fluid Mech.* **6**, 161–205.

BENJAMIN, T. B. 1960 Effects of a flexible boundary on hydrodynamic stability. *J. Fluid Mech.* **9**, 513–532.

BENJAMIN, T. B. 1963 The threefold classification of unstable disturbances in flexible surfaces bounding inviscid flows. *J. Fluid Mech.* **16**, 436–450.

BENJAMIN, T. B. 1964 Fluid flow with flexible boundaries. In *Proc. 11th Intl Congr. Appl. Maths., Munich, Germany* (ed. H. Görtler), p. 109. Springer.

BRAZIER-SMITH, P. R. & SCOTT, J. F. 1984 Stability of fluid flow in the presence of a compliant surface. *Wave Motion* **6**, 547–560.

BRIGGS, R. J. 1964 *Electron-Stream Interaction with Plasmas*. M.I.T. Press.

CAIRNS, R. A. 1979 The role of negative energy waves in some instabilities of parallel flows. *J. Fluid Mech.* **92**, 1–14.

CARPENTER, P. W. 1984*a* The effects of damping on the hydrodynamic stability of flows over Kramer-type compliant surfaces. in *Laminar/Turbulent Boundary Layers* (ed. E. M. Uram & H. E. Weber), pp. 53–59. ASME.

CARPENTER, P. W. 1984*b* The effect of a boundary layer on the hydroelastic instability of infinitely long plates. *J. Sound Vib.* **93**, 461–464.

CARPENTER, P. W. 1984*c* A note on the hydroelastic instability of orthotropic panels. *J. Sound Vib.* **94**, 553–554.

CARPENTER, P. W. & GARRAD, A. D. 1982 Effect of a viscous fluid substrate on the flow-induced vibrations of a compliant coating. In *Proc. Intl Conf. on Flow Induced Vibrations in Fluid Engineering* (ed. H. S. Stephens & G. B. Warren), pp. 369–382. BHRA Fluid Engineering, Cranfield, England.

CARPENTER, P. W. & GARRAD, A. D. 1985 The hydrodynamic stability of flows over Kramer-type compliant surfaces. Part 1. Tollmien–Schlichting instabilities. *J. Fluid Mech.* **155**, 465–510.

CARPENTER, P. W., GASTER, M. & WILLIS, G. J. K. 1983 A numerical investigation into boundary layer stability on compliant surfaces. In *Numerical Methods in Laminar and Turbulent Flow*, pp. 166–172. Pineridge.

DOWELL, E. H. 1971 Generalised aerodynamic forces on a flexible plate undergoing transient motion in a shear flow with an application to panel flutter. *AIAA J.* **9**, 834–841.

DOWELL, E. H. 1975 *Aero-elasticity of Plates and Shells*. Noordhoff.

DOWELL, E. H. 1985 The effects of compliant walls on transition and turbulence. In *Proc. Symp. on Shear Flow–Structure Interaction Phenomena, November* 1985, pp. 37–52. ASME.

DUGUNDJI, J., DOWELL, E. & PERKIN, B. 1963 Subsonic flutter of panels on a continuous elastic foundation. *AIAA J.* **1**, 1146–1154.

DUNCAN, J. H., WAXMAN, A. M. & TULIN, M. P. 1985 The dynamics of waves at the interface between a visco-elastic coating and a fluid flow. *J. Fluid Mech.* **158**, 177–197.

ESSAPIAN, F. S. 1955 Speed-induced skin folds in the bottle-nosed porpoise, Tursiops Truncatus. *Breviora Mus. Comp. Zool.* **43**, 1–4.

FRASER, L. A. & CARPENTER, P. W. 1985 A numerical investigation of hydroelastic and hydrodynamic instabilities in laminar flows over compliant surfaces comprising one or two layers of visco-elastic material. In *Numerical Methods in Laminar and Turbulent Flow*, pp. 1171–1181. Pineridge.

GAD-EL-HAK, M. 1985 Stability of compliant surfaces. Presentation at *Drag Reduction & Boundary Layer Control Symp., Oct.* 1985. Nat. Acad. Sci., Washington, D.C.

GAD-EL-HAK, M. 1986*a* The response of elastic and visco-elastic surfaces to a turbulent boundary layer. *Trans. ASME* E: *J. Appl. Mech.* **53**, 206–212.

GAD-EL-HAK, M. 1986*b* Boundary layer interactions with compliant coatings: An overview. *Appl. Mech. Rev.* **39**, 511–523.

GAD-EL-HAK, M., BLACKWELDER, R. F. & RILEY, J. J. 1984 On the interaction of compliant coatings with boundary-layer flows. *J. Fluid Mech.* **140**, 257–280.

GARRAD, A. D. & CARPENTER, P. W. 1982*a* On the aerodynamic forces involved in aeroelastic instability of two-dimensional panels in uniform incompressible flow. *J. Sound Vib.* **80**, 437–439.

GARRAD, A. D. & CARPENTER, P. W. 1982*b* A theoretical investigation of flow-induced instabilities in compliant coatings. *J. Sound Vib.* **85**, 483–500.

GASTER, M. 1962 A note on the relation between temporally-increasing and spatially-increasing disturbances in hydrodynamic stability. *J. Fluid Mech.* **14**, 222–224.

GASTER, M. 1965*a* On the generation of spatially growing waves in a boundary layer. *J. Fluid Mech.* **22**, 433–441.

GASTER, M. 1965*b* The role of spatially growing waves in the theory of hydrodynamic stability. *Prog. Aero. Sci.* **6**, 251–270.

GASTER, M. 1968 Growth of disturbances in both space and time. *Phys. Fluids* **11**, 723–727.

GASTER, M. & WILLIS, G. J. K. 1984 A rapid eigenvalue finder for flows over a compliant surface. In *Laminar/Turbulent Boundary Layers* (ed. E. M. Uram & H. E. Weber), pp. 79–84. ASME.

HANSEN, R. J. & HUNSTON, D. L. 1974 An experimental study of turbulent flows over compliant surfaces. *J. Sound Vib.* **34**, 297–308.

HANSEN, R. J. & HUNSTON, D. L. 1976 Further observations on flow-generated surface waves in compliant surfaces. *J. Sound Vib.* **46**, 593–595.

HANSEN, R. J. & HUNSTON, D. L. 1983 Fluid-property effects on flow-generated waves on a compliant surface. *J. Fluid Mech.* **133**, 161–177.

HANSEN, R. J., HUNSTON, D. L., NI, C. C. & REISCHMANN, M. M. 1980*a* An experimental study of flow-generated waves on a flexible surface. *J. Sound Vib.* **68**, 317–334.

HANSEN, R. J., HUNSTON, D. L., NI, C. C., REISCHMANN, M. M. & HOYT, J. W. 1980*b* Hydrodynamic drag and surface deformations generated by liquid flows over flexible surfaces. In *Viscous Flow Drag Reduction* (ed. G. R. Hough), pp. 439–452. *AIAA.* Prog. Astro. Aero., vol. 72.

HERTEL, H. 1963 *Structure – Form – Movement.* Reinhold.

KORNECKI, A. 1978 Aeroelastic and hydroelastic instabilities of infinitely long plates. I. *Solid Mech. Arch.* **3**, 381–440.

KORNECKI, A., DOWELL, E. H. & O'BRIEN, J. 1976 On the aeroelastic instability of two-dimensional panels in uniform incompressible flow. *J. Sound Vib.* **47**, 163–178.

KRAMER, M. O. 1960 Boundary layer stabilization by distributed damping. *J. Am. Soc. Nav. Engrs.* **72**, 25–33.

LANDAHL, M. T. 1962 On the stability of a laminar incompressible boundary layer over a flexible surface. *J. Fluid Mech.* **13**, 609–632.

LANDAHL, M. T. 1964 Graphical technique for analysing marginally stable dynamic systems. *J. Aircraft* **1**, 293–299.

LANDAHL, M. T. & KAPLAN, R. E. 1965 Effect of compliant walls on boundary layer stability and transition. *AGARDograph* 97-1-353.

MACMICHAEL, J. M., KLEBANOFF, P. S. & MEASE, N. E. 1980 Experimental investigation of drag on a compliant surface. In *Viscous Flow Drag Reduction* (ed. G. R. Hough), pp. 410–438. *AIAA.* Prog. Astro. Aero., vol. 72.

MELCHER, J. R. 1981 *Continuum Electromechanics.* M.I.T. Press.

MILES, J. W. 1957 On the generation of surface waves by shear flows. *J. Fluid Mech.* **3**, 185–199.

MILES, J. W. 1959*a* On the generation of surface waves by shear flows. Part 2. *J. Fluid Mech.* **6**, 568–582.

MILES, J. W. 1959*b* On the generation of surface waves by shear flows. Part 3. Kelvin–Helmholtz instability. *J. Fluid Mech.* **6**, 583–598.

MILES, J. W. 1962 On the generation of surface waves by shear flows. Part 4. *J. Fluid Mech.* **13**, 433–448.

NISEWANGER, C. R. 1964 Flow noise and drag measurements of vehicle with compliant coating. *U.S. Naval Ordnance Test Station, China Lake, California. NAVWEPS Rep.* 8518.

PURYEAR, F. W. 1962 Boundary layer control drag reduction by compliant surfaces. *U.S. Dept. of Navy, David Taylor Model Basin. Rep.* 1668.

RITTER, H. & MESSUM, L. T. 1964 Water tunnel measurements of turbulent skin friction on six different compliant surfaces of one foot length. *Admiralty Research Lab. Rep.* ARL/G/N9.

RITTER, H. & PORTEOUS, J. S. 1965 Water tunnel measurements of skin friction on a compliant coating. *Admiralty Research Lab. Rep.* ARL/N3/G/HY/9/7.

SCHUBAUER, G. B. & SKRAMSTAD, H. K. 1948 Laminar boundary layer oscillations and transition on a flat plate. *NACA Rep.* 909.

WEAVER, D. S. & UNNY, T. E. 1970 The hydroelastic stability of a flat plate. *Trans. ASME* E: *J. Appl. Mech.* **37**, 823–827.